Development 140, 2253-2268 (2013) doi:10.1242/dev.079111

Polar auxin transport: models and mechanisms

Klaartje van Berkel[1,2,*,‡], Rob J. de Boer[2], Ben Scheres[1,*] and Kirsten ten Tusscher[2,‡]

Summary

Spatial patterns of the hormone auxin are important drivers of plant development. The observed feedback between the active, directed transport that generates auxin patterns and the auxin distribution that influences transport orientation has rendered this a popular subject for modelling studies. Here we propose a new mathematical framework for the analysis of polar auxin transport and present a detailed mathematical analysis of published models. We show that most models allow for self-organised patterning for similar biological assumptions, and find that the pattern generated is typically unidirectional, unless additional assumptions or mechanisms are incorporated. Our analysis thus suggests that current models cannot explain the bidirectional fountain-type patterns found in plant meristems in a fully self-organised manner, and we discuss future research directions to address the gaps in our understanding of auxin transport mechanisms.

Key words: Computer simulation, Mathematical biology, Plant hormone

Introduction

Polar auxin transport

The plant hormone auxin plays a crucial role in the spatiotemporal control of plant development, and its patterns of distribution and activity must be tightly regulated. For example, in the root meristem a gradient of auxin with its maximum in the root tip determines the location of the quiescent centre and surrounding stem cells (Sabatini et al., 1999) and the regions where cell division, expansion and differentiation occur. Local maxima of auxin in the shoot apical meristem and in the differentiation zone of the mature root guide primordium outgrowth (Casimiro et al., 2001; Reinhardt et al., 2000), while in leaves, streams of auxin precede vein formation (Scarpella et al., 2006).

Much of the spatial distribution of auxin is caused by directional transport [polar auxin transport (PAT); see Glossary, Box 1]. The low pH in cell walls causes auxin to become protonated, allowing it to enter cells relatively easily. In addition, influx carriers of the AUX/LAX family pump auxin into cells. Owing to the higher pH in the cytosol, cellular auxin loses its ability to cross the membrane. Thus, auxin needs to be actively pumped out of cells by efflux carriers. Proteins of the PIN-FORMED (PIN) family are an important group of efflux carriers (Gälweiler et al., 1998; Muller et al., 1998, Paponov et al., 2005; Friml, 2003). They typically have a polar cellular distribution, leading to directed auxin transport across only those membranes where PINs are localised (hereafter, we describe PINs as 'pointing' in the direction along which auxin

[1]Molecular Genetics Group and [2]Theoretical Biology Group, Department of Biology, Utrecht University, Padualaan 8, 3584 CH Utrecht, The Netherlands.

*Present address: Wageningen University Research, Droevendaalsesteeg 1, 6708 PB Wageningen, The Netherlands
‡Authors for correspondence (k.vanberkel@uu.nl; k.h.w.j.tentusscher@uu.nl)

Box 1. Glossary

Cell polarity. The cell has two distinct equilibria in which PIN levels are high on one membrane segment and low on the opposite membrane segment.
Equilibrium. Intersection point of two equilibrium lines in the phase plane, where both variables of the system are in steady-state (i.e. do not change their value).
Equilibrium line. Connected series of points in the phase plane for which one of the system variables is in steady-state.
Feedback. Effect of an input variable or process (e.g. auxin level or auxin flux) on an output variable or process (e.g. PIN level or PIN cycling dynamics).
Gradient-driven amplification. Amplification of a persistent gradient prepattern due to positive feedback (self-amplification).
Linear feedback. Linearly proportionate effect of input auxin levels or fluxes (x) on output PIN levels or dynamics (y): $y=ax$.
Maximal self-organising potential. The most autonomous pattern formation a system is able to generate, with self-organisation being more autonomous than self-amplification.
Mechanistic feedback. Feedback rules based on molecular data (bottom-up) as opposed to tissue level observations (top-down).
Membrane bistability. The membrane has two distinct, stable equilibria in which the PIN concentration is either high or low.
Phase plane. Graph that represents the dynamics of two interdependent variables, containing equilibrium lines, equilibrium points and vectors.
Polar auxin transport (PAT). The auxin transport that is mediated by polarly localised PIN proteins.
Polarity-driven self-organisation. The ability to self-organise patterns as a result of feedback mechanisms producing cell polarity.
Superlinear (or supralinear) feedback. A more than linearly proportionate effect of input auxin levels or fluxes (x) on output PIN levels or dynamics (y): $y=ax^n$, with $n>1$ (if $n=2$ the feedback is termed quadratic).
Saturating (or saturated) feedback. A feedback function in which the amount of increase of output (y) with increases in input (x) declines when input levels are higher, until output no longer increases when input level increases. $y=ax/(h+x)$ represents a linear saturated feedback, whereas $y=ax^n/(h^n+x^n)$ with $n>1$ represents a superlinear saturated feedback.
Self-amplification. Amplification of the differences present in a persistent prepattern due to positive feedback.
Self-organisation. The ability to generate patterns from a transient perturbation and maintain patterns without the presence of a persistent prepattern.
Stable equilibrium. An equilibrium to which the state of the dynamic system converges, resulting in a constant concentration of the variables of the system defined by the location of the equilibrium.
Turing-type pattern formation. Persistent pattern formation due to local activation and global inhibition, resulting in spot or stripe patterns.
Unstable equilibrium. Equilibrium from which the state of the dynamic system diverges, resulting in a change of variables away from the values defined by the location of the equilibrium.

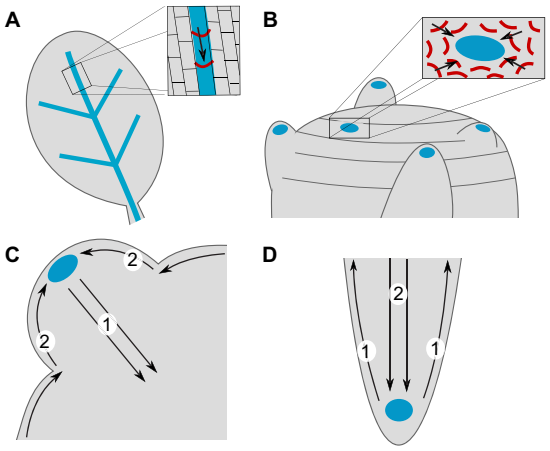

Fig. 1. Schematic representations of PIN and auxin patterns in different plant tissues. Auxin is in blue and PIN proteins in red; arrows indicate the direction of auxin flux. (**A**) Auxin-accumulating veins in a developing leaf. (Inset) PIN proteins point with the flux of auxin toward the base of the leaf. (**B**) Phyllotaxy pattern on the shoot apical meristem, where auxin maxima precede primordia and form in a regular pattern. (Inset) PIN proteins point toward each auxin maximum. (**C**) Reverse-fountain-like pattern in a developing shoot primordium. In the inner layers, PINs transport auxin away from the maximum (direction 1), whereas in the outer layer, PINs transport auxin toward the maximum (direction 2). (**D**) Fountain-like pattern in the root tip. PINs in the outer layer transport auxin away from the maximum (direction 1), whereas PINs in the inner layers transport auxin toward the maximum (direction 2).

flow is induced by the PIN distribution). This polar localisation depends on both developmental conditions and cell type (Petrášek et al., 2006; Wisniewska et al., 2006). In leaves, cell files with polar PIN distributions generate auxin-transporting veins (Fig. 1A), whereas in the epidermis of the shoot apical meristem PINs point toward the different auxin maxima that demarcate subsequent incipient primordia, thus producing phyllotactic patterns (Fig. 1B) (Reinhardt et al., 2003). Within these individual shoot primordia, PINs in the outer tissue layers are localised toward the auxin maximum in the primordium tip, whereas inner layers form veins with PINs pointing away from the maximum, connecting the primordium to the vasculature (Fig. 1C) – a pattern known as a reverse-fountain. Finally, in the root tip and lateral root primordia, an opposite PIN pattern (whereby PINs in the outer layers transport auxin away from the local maximum, whereas inner files of cells direct auxin towards the maximum) is observed (Fig. 1D), and this is referred to as a fountain (Blilou et al., 2005). Mathematical models for the root (Grieneisen et al., 2007) and shoot (de Reuille et al., 2006) meristem have demonstrated that the experimentally observed PIN polarity patterns are both necessary and sufficient for the correct build-up of auxin maxima.

PIN proteins undergo constant cycling to and from the plasma membrane (PM) (Geldner et al., 2001; Dhonukshe et al., 2007), allowing them to dynamically maintain their polarity and to quickly redistribute in response to endogenous triggers (primordia formation, gravitropic response) or external stimuli (wounding, stretching). It has been experimentally shown that externally applied auxin can induce new primordia (Reinhardt et al., 2000; Reinhardt et al., 2003), indicating its ability to alter the polar distribution of PIN proteins and thus implying a feedback (see Glossary, Box 1) loop between auxin and its own transport. As PIN proteins constantly cycle to and from the PM, it is likely that this feedback represents a regulatory effect of auxin on PIN cycling. Indeed, it has been shown (Paciorek et al., 2005; Robert et al., 2010) that ectopically added auxin counteracts the PIN internalisation induced by the exocytosis-inhibiting drug BFA, and this has been interpreted as an inhibitory effect of auxin on endocytosis. However, it is currently hard to establish whether intra- or extracellular auxin or auxin flux is affecting PIN cycling in these experiments, and whether cells sense auxin directly or also indirectly via mechanosensitive signalling pathways.

PAT models

Long before the discovery of PIN proteins and the auxin dependence of their polar localisation, it was already hypothesised that auxin positively influences its own transport and spatial distribution, implying that auxin patterning might be self-amplifying and potentially even self-organising (Sachs, 1969). It is this implication that served as a major inspiration for the numerous modelling studies in this area. In the case of self-amplification (see Glossary, Box 1), the plant is capable of responding to and enhancing a superimposed auxin prepattern, for example a local source or sink, but requires this prepattern to persist. By contrast, in the case of self-organisation (see Glossary, Box 1), a transient prepattern is sufficient for initialisation and subsequent autonomous maintenance of the formed pattern.

Owing to the current lack of a fully mechanistic molecular understanding of how cells sense auxin and how this subsequently influences PIN polarity and auxin transport, most current models have taken a top-down approach, correlating the observed auxin and PIN polarity patterns in the tissue of interest to derive a hypothetical feedback mechanism. Based on their proposed feedback mechanism, PAT models can be divided into two main classes: flux-based and concentration-based models.

Flux-based models are based on Sachs' canalisation hypothesis (Sachs, 1969), which states that cells experiencing flux of a molecule in a certain direction will increase their capacity to transport the molecule in that direction, and is based on the observation that, during vein formation, auxin transport channels become gradually more distinct. The auxin transport capacity is represented by membrane permeability in early models (Mitchison, 1980; Mitchison, 1981) and by membrane PIN concentration in later models (e.g. Fujita and Mochizuki, 2006; Feugier and Iwasa, 2006; Alim and Frey, 2010; Feugier et al., 2005; Stoma et al., 2008). Flux-based models have mainly been used to model venation patterns, and demonstrate that small fluctuations in auxin may be amplified into more distinct streams, with PINs pointing in the direction of the flux, i.e. with-the-flux (Fig. 1A, inset).

Concentration-based models (e.g. Smith et al., 2006; Newell et al., 2007; Jönsson et al., 2006; Merks et al., 2007) were formulated after the discovery of PIN proteins and therefore all explicitly model membrane PIN levels. In these models, PIN levels increase on the membrane facing the neighbouring cell with the highest auxin level, i.e. up-the-gradient. This proposed feedback mechanism was inspired by observations in the shoot apex, where PINs in the epidermal layer orient toward local auxin maxima that develop into organ primordia (Fig. 1B, inset) (Reinhardt et al., 2003). Concentration-based models are sufficient to obtain phyllotaxis-like patterns by amplifying small local increases in auxin into distinct maxima while simultaneously depleting neighbouring cells, resulting in the occurrence of new maxima at fixed distances from older maxima.

More recently, efforts have been made to construct PAT models capable of displaying both up-the-gradient phyllotaxis and with-

the-flux venation types of PIN patterning (Bayer et al., 2009; Merks et al., 2007; Stoma et al., 2008) in order to explain reverse-fountain-type patterns (Fig. 1C). Additionally, somewhat more mechanistic feedback (see Glossary, Box 1) loops of auxin on PAT have been suggested. Based on the observation that PIN polarity correlates with stress-related microtubule alignment, a model has been proposed in which auxin influences wall stress, which in turn influences PIN localisation (Heisler et al., 2010). Alternatively, it has been proposed that PIN polarity is regulated by auxin receptors in the apoplast, which inhibit local PIN endocytosis after binding auxin (Wabnik et al., 2010).

A framework to analyse and compare PAT models

In this Hypothesis we will perform a detailed comparison and analysis of a broad range of models for auxin patterning in plant development. For flexible developmental patterning, the feedback between active polar auxin transport, which generates auxin distribution patterns, and these auxin distributions in turn shaping the strength and direction of this polar auxin transport, is crucial. Therefore, we restrict this analysis to models that incorporate polar auxin transport and its auxin-dependent regulation, focusing on both the auxin and PIN distribution patterns that are generated. Thus, we will not include strictly mechanical models that do not consider feedback on auxin transport, Turing-type models (see Glossary, Box 1) in which only passive undirected auxin transport is considered, or models in which the directions of active PAT are assumed to be constant (e.g. Grieneisen et al., 2007).

One straightforward way to evaluate and compare the various PAT models is by analysing the tissue level auxin and PIN patterns that they generate and compare these with experimental data. A number of excellent reviews have been written that describe these efforts (Wabnik et al., 2011; Heisler and Jönsson, 2006; Kramer, 2009; Garnett et al., 2010). However, for a mathematical model to work, detailed specifications have to be made for the dynamics on the subcellular membrane segment, cellular and tissue levels. Indeed, apart from the simple dichotomy in concentration and flux-based models, a variety of mathematical formulations for processes such as PIN-mediated auxin pumping, PIN dynamics and auxin-PIN feedback functions are used in the different models, the precise relevance of which is not trivial for even the experienced modeller. Therefore, as recently pointed out in a review by Jönsson and Krupinski (Jönsson and Krupinski, 2010), it is of crucial importance to develop a general framework to analyse and compare these different mathematical formulations, classify them into a limited number of corresponding biological assumptions, and determine how these influence model patterning behaviour.

Another crucial aspect is to determine the extent to which the model generates these patterns in an autonomous self-organised manner. Although self-organising and self-amplifying models may produce similar spatial patterns, whether this patterning requires a persistent prepattern is of key relevance. If auxin patterning required a prepattern, then a mechanism would be needed to explain the generation of these prepatterns. Furthermore, changes in auxin patterns precede major changes in the expression of developmental genes and cell morphology. Thus, for plants to keep generating new organs robustly throughout their life, it seems essential that the new auxin patterns required by each newly forming organ primordium arise in a largely self-organised manner independently of a prepattern.

In this Hypothesis we develop a general mathematical and simulation framework in which we analyse and compare most currently published PAT models. We translate the various mathematical formulations that are used into biological assumptions, and analyse how these relate to model behaviour, investigating both the type of auxin patterns generated and to what extent these are fully self-organised. We restrict our analysis to assumptions regarding PIN-mediated auxin transport dynamics, PIN cycling and auxin-PIN polarisation feedback, assuming these to be the main determinants for auxin patterning. The transcriptional effect of auxin on PIN expression levels (Vieten et al., 2005) is

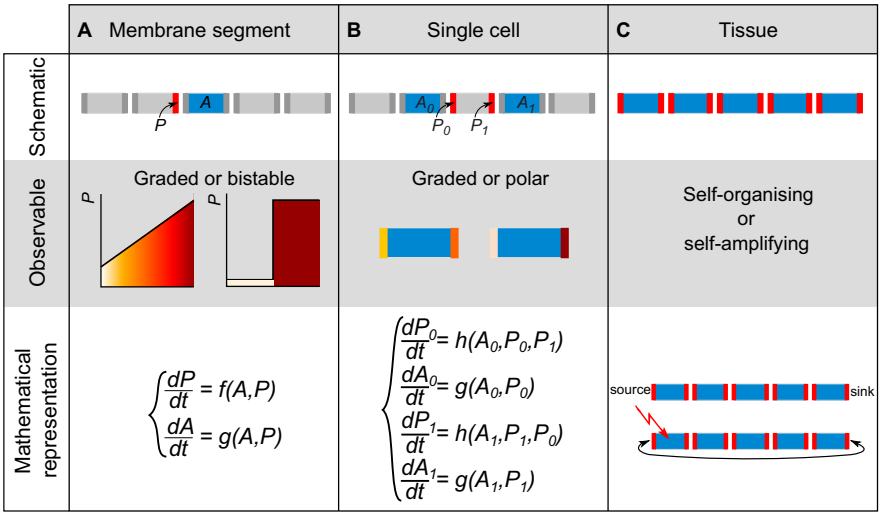

Fig. 2. Mathematical framework to study PAT models. (**A**) At the membrane segment level, we focus on the PIN concentration (ranging from white for low to red for high) at a membrane segment (*P*) and the auxin concentration (blue) in the adjoining neighbouring cell (*A*). The resulting system of two equations is used to investigate whether the model allows for bistability at the membrane segment level. (**B**) The single-cell model is constructed from two membrane segments. The result is a four-variable model system, describing the PIN concentrations at the cell's two membrane segments (P_0 and P_1) and the corresponding auxin concentrations in both neighbouring cells (A_0 and A_1). The focus is on whether a cell can be polar. (**C**) A tissue is formed by combining five cells into a file flanked by a source and a sink, or by forming a closed ring, in order to model tissue level patterning behaviour with respect to a persistent global gradient (formed through the presence of a source and sink), or a transient perturbation in the auxin level of a single cell (red arrow), respectively. We focus on whether the model is self-organised.

mostly ignored because the short-term effect of auxin on PIN polarisation is expected to be more important for the self-organising capabilities of a mechanism than the long-term effect of auxin on overall PIN levels. Model behaviour will be analysed with regard to three levels of increasing complexity: the membrane segment, single-cell and one-dimensional (1D) tissue levels (Fig. 2A-C, respectively). Our 1D tissue level analysis does not allow us to directly determine the type of 2D or 3D patterns that a model can generate. However, it allows us to determine whether PINs orient away or toward an auxin maximum and whether a single mechanism can generate the two opposite polarisation patterns observed in fountain-type patterns. Additionally, we can establish a model's self-organising potential in simple 1D tissue simulations. If a model generates self-organised patterns in one dimension, it will also do so in two or three dimensions. Thus, we can still extrapolate our 1D results to qualitatively predict the extent to which a model can generate complex tissue patterns, such as fountain-like patterns, and to what extent this patterning might be self-organised.

Our analysis will demonstrate that most published models are capable of producing robust, self-organised auxin and PIN patterns, and that flux-based and concentration-based models achieve this with largely similar biological assumptions. It appears that flux-based models are somewhat more versatile in explaining different PIN orientations, but both model categories seem to have difficulties in explaining the bidirectional fountain-type patterns observed *in planta* in a fully self-organised manner. We thus conclude that none of the currently available models robustly produces fountain-like patterns by a single mechanism. Finally, future directions for research are recommended in order to close in on the mechanistic basis of auxin feedback in plants and determine how fountain-type patterns are generated.

Model behaviour on three levels of organisation

In the following sections, published PAT models will be compared in terms of the mathematical formulations used for PIN-mediated auxin pumping dynamics, PIN cycling and auxin-PIN feedback, the biological assumptions to which these correspond, and the resulting model behaviour on the membrane segment, single-cell and tissue levels. A major goal of our analysis is to determine the maximal self-organising potential (see Glossary, Box 1) of models and the mathematical and biological assumptions on which this potential critically depends. As model behaviour depends both on mathematical formulations and parameter settings, we will classify a model as self-organising if self-organising patterns occur in at least a region of parameter space. We will first analyse in detail two representative examples of PAT models (chosen solely to facilitate discussion of our analysis of self-organising properties), following which we apply the same evaluation to a broader range of published models.

We have developed a generalised mathematical framework to study model assumptions and resulting behaviour (Fig. 2). In our analysis, the original mathematical formulation and biological assumptions of the discussed models are followed, but some simplifications are used to allow for an analytical approach. For ease of comparison we introduce a single set of variable and parameter names used for all models, rather than adopting the different names used in the various publications (see Table 1 for these parameters and variables, their biological meanings and default values). An in-depth description of the mathematical framework is provided in supplementary material Appendix S1.

We start with a simplified model at the membrane segment level and extend this first to the single-cell and subsequently to the 1D tissue level. Boxes 2 and 3 explain the mathematical formulation and analysis of the membrane segment and single-cell models. With regard to membrane segments, we are interested in whether the model allows for two alternative stable equilibria (see Glossary, Box 1) – termed membrane bistability (see Glossary, Box 1) – in which case membrane segments have either a discrete high or low PIN level. Alternatively, membrane segments may have a single equilibrium PIN level, in which case the PIN levels on a membrane segment may vary only according to locally experienced auxin levels that influence the precise location of this equilibrium ('graded distribution') (Fig. 2A).

At the cell level we are interested in whether the model allows for stable equilibria in which a cell has a distinct high PIN level on one membrane segment and a distinct low PIN level on the

Table 1. Frequently used variables and parameters, their biological meanings, units and default values

Variable	Biological meaning	Units
P_i	PIN concentration on membrane segment of interest	[]
A_i	Auxin concentration in neighbouring cell of interest	[]
F	Auxin flux over membrane segment of interest into neighbouring cell of interest	$[]s^{-1}$
Parameter	**Biological meaning**	**Units and default values**
p	Auxin production	$1\ []s^{-1}$
d	Auxin decay	$0.5\ s^{-1}$
i_{pas}	Passive influx over the membrane segment of interest into the neighbouring cell of interest	$0.01\ []s^{-1}$
i_{pin}	PIN-mediated influx over the membrane segment of interest into the neighbouring cell of interest	$1\ s^{-1}[]^{-1}$
e	Total efflux out of the neighbouring cell of interest over the membrane segment of interest	$1\ s^{-1}$
e_{pas}	Passive efflux out of the neighbouring cell of interest over the membrane segment of interest	$0.01\ s^{-1}$
e_{pin}	PIN-mediated efflux out of the neighbouring cell of interest over the membrane segment of interest	$1\ s^{-1}[]^{-1}$
k_{on}	PIN exocytosis/recycling rate	–
k_{on_b}	Basal exocytosis/recycling rate	$0.01\ s^{-1}$
k_{on_f}	Auxin-dependent exocytosis/recycling rate	$1\ s^{-1}$
k_{off}	PIN endocytosis rate	$1\ s^{-1}$
k_{off_b}	Basal endocytosis rate	–
k_{off_f}	Auxin-dependent endocytosis rate	–
P_{tot}	The total amount of PINs in one cell	10 []

Note that under default conditions feedback is on k_{on}, with k_{off} constant. Consequently, k_{on} is not defined as a constant value, but is instead a function of k_{on_b}, k_{on_f} and auxin level or flux, while k_{off} has a defined constant value and k_{off_b} and k_{off_f} are not defined. If, instead, feedback is on k_{off} the situation is reversed. [] is used for concentration.

Box 2. The membrane segment

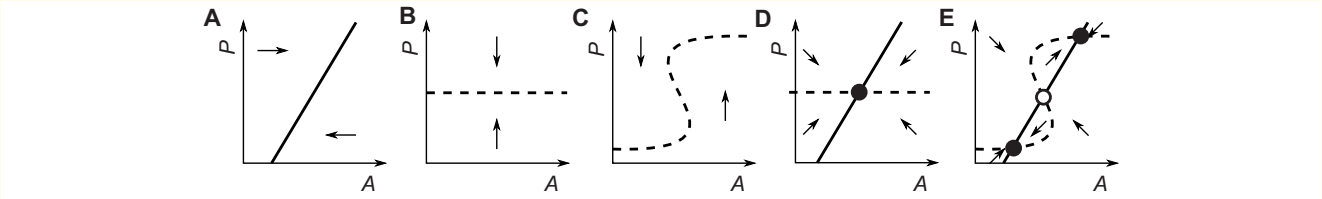

At the membrane segment level, we take into account the model's description of PIN (*P*) dynamics on a single membrane segment and auxin concentration (*A*) in the adjoining neighbouring cell (see Fig. 2). Other PIN and auxin concentrations are assumed to be constant, which constitutes a mathematical tool enabling our membrane level analysis by limiting the number of variables included in the model, rather than a biological assumption; indeed, as we move in our analysis to the single-cell and tissue level these concentrations are no longer assumed constant. As we do not explicitly model the cell wall, the efflux over the membrane segment equals the influx into the neighbouring cell and vice versa. Hence, we can write for the auxin concentration:

$$\frac{dA}{dt} = p + i_{pas} + i_{pin}P - eA - dA\,, \quad (1)$$

with parameter symbols, meanings and default values described in Table 2.

Eq. 2 describes the auxin equilibrium line, which is the series of points (*A*,*P*) for which the auxin concentration is in equilibrium (*dA*/*dt*=0):

$$P = \frac{(e+d)A - p - i_{pas}}{i_{pin}}\,, \quad (2)$$

which is the solid line in panel A. To the left of the equilibrium line, net influx occurs and auxin increases (→), whereas to the right, auxin decreases due to net efflux (←).

Taking into consideration the dynamic cycling of PIN proteins between membrane and cytosol, we can model membrane segment PIN levels as:

$$\frac{dP}{dt} = k_{on} - k_{off}P\,. \quad (3)$$

If k_{on} and k_{off} are constant (no feedback), the equilibrium line for PINs (*dP*/*dt*=0) is given by $P=k_{on}/k_{off}$ (dashed line in B). Above this line, PINs decrease (↓), whereas below this line they increase (↑). A positive feedback of auxin flux or concentration on PIN levels is incorporated by allowing the auxin flux or level to either increase k_{on} or decrease k_{off}. This dependence of k_{on} or k_{off} on auxin can be modelled using either a linear feedback (e.g. $y=ax$), a superlinear feedback (e.g. $y=ax^n$), a (sub)linear saturating feedback [e.g. $y=ax/(h+x)$] or a superlinear saturating feedback [e.g. $y=ax^n/(h^n+x^n)$], depending on the assumed effect of auxin on PIN cycling dynamics (with *a* and *h* being arbitrary scaling parameters and *n* a measure of cooperativity). A hypothetical PIN equilibrium line resulting from a saturating superlinear feedback is given in C.

In D and E the auxin equilibrium line and auxin dynamics are drawn together with the two PIN equilibrium lines and PIN dynamics, allowing us to assess the overall behaviour of the membrane segment model. In the figures we can find the system's equilibrium points (circles), in which both *dA*/*dt*=0 and *dP*/*dt*=0 and hence no changes occur, as intersection points of the *A* and *P* equilibrium lines. In addition, we can determine the stability of the equilibria from the direction of the dynamics (arrows) near an equilibrium. An equilibrium is stable if all arrows point toward it (black circles), whereas an equilibrium is unstable if one or more arrows point away from it (white circles). In D, the system has a single stable equilibrium. In E, the system has three equilibria, the middle one being unstable and the outer two stable, and thus represents a bistable membrane segment system.

opposing membrane segment, thus allowing for cell polarity (see Glossary, Box 1) (Fig. 2B). In the absence of such cell polarity, opposing membranes will only display different PIN levels if persistently different auxin levels are present near both membranes. We analyse and discuss the relationship between membrane segment bistability and cell level polarity.

Tissue level behaviour is analysed using a 1D array of five cells (Fig. 2C). First, the cells are organised as a file with a source of auxin at one end and a sink at the other. This allows us to test whether cells polarise and to determine the direction of polarity with respect to the global auxin gradient (i.e. the type of pattern formed) (Fig. 2C). Second, the file is wrapped into a ring, and a transient increase in the auxin level of a single cell is applied. In this system, we can investigate whether a transient perturbation spreads out and leads to persistent patterning or dies out, causing the tissue to return to its uniform state. If persistent pattern formation occurs in both configurations (file and ring) the tissue pattern is self-organising. If patterning is self-organised and driven by lower level membrane bistability and cell polarity, we will name it polarity-driven self-organisation (see Glossary, Box 1) to distinguish it from more conventional and well-analysed Turing-like self-organised patterning. If patterning is not self-organised and is instead maintained only in the presence of sources and sinks, the pattern formation is considered as gradient-driven amplification (see Glossary, Box 1), i.e. to be self-amplifying.

Analysis of published models

Example 1: flux-based model

Stoma et al. (Stoma et al., 2008) developed a flux-based PAT model in which the PIN concentration at a given membrane segment is assumed to increase with the net efflux of auxin over that membrane segment. Both linear and quadratic feedback functions for the dependence of PIN levels on auxin were used. Linear feedback (see Glossary, Box 1) implies that similar flux increases cause similar PIN level increases independently of the flux level. By contrast, superlinear (e.g. in this case quadratic) feedback (see Glossary, Box 1) implies that similar flux increases cause larger PIN increases for higher flux levels. The authors furthermore assumed that the availability of PIN proteins within a single cell is never limiting, i.e. the allocation of PINs to membrane segments does not lower the amount of PINs available for exocytosis/recycling sufficiently to cause competition between membrane segments. Finally, pumping of auxin by PIN proteins is assumed to depend linearly on intracellular auxin concentrations. In biological terms this assumption requires that PIN proteins are sufficiently available to handle large auxin concentrations and are thus not limiting for the rate of flux.

Box 3. The single cell

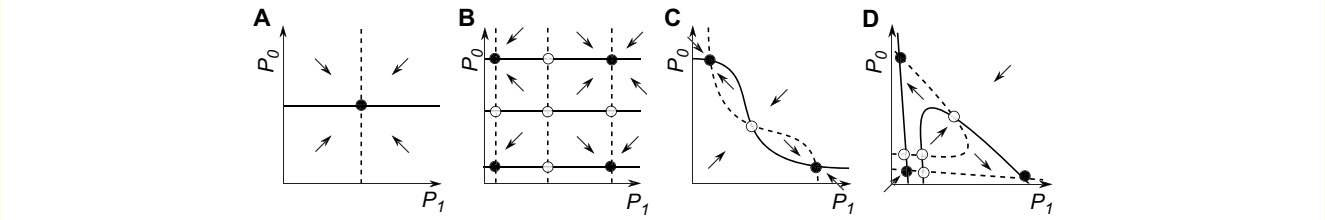

To model a single cell in a simplified manner we consider the PIN levels on the two opposing membrane segments of the cell (P_0 and P_1) and the auxin concentrations in the two neighbouring cells (A_0 and A_1) (see Fig. 2). Again, we assume other auxin and PIN concentrations to be constant. The cell level model thus can be written as:

$$\frac{dA_i}{dt} = p + i_{pas} + i_{pin}P_i - eA_i - dA_i \,, \tag{4a}$$

$$\frac{dP_i}{dt} = k_{on_i} - k_{off_i}P_i \,, \tag{4b}$$

with i=0 or 1.

If, in a model, a limiting PIN pool is assumed, the equation for P_i becomes:

$$\frac{dP_i}{dt} = k_{on_i}(P_{tot} - P_0 - P_1) - k_{off_i}P_i \,. \tag{5}$$

The recycling rate now depends on the amount of available PINs in the cytosol, which is the total amount of PINs per cell (P_{tot}) minus the PINs that are bound to membrane segments.

To simplify the system and allow for 2D phase plane (see Glossary, Box 1) analysis, we make a quasi-steady-state assumption by letting the auxin dynamics at all times be in equilibrium with the amount of PINs at the membrane segment (dA_i/dt=0). This assumption does not alter the model behaviour in which we are interested, namely the number of equilibria. Hence, the expression for A_i becomes:

$$A_i = \frac{p + i_{pas} + i_{pin}P_i}{e + d} \,. \tag{6}$$

This leaves us with two equations for the PINs (Eq. 4b or Eq. 5) in which either k_{on} or k_{off} rates depend on auxin flux or concentration and hence on the equilibrium values of auxin given by Eq. 6.

The behaviour of the cell model depends both on the behaviour of the model at the membrane segment level and on whether a limiting PIN pool is assumed. If the PIN pool is non-limiting, P_0 and P_1 are completely independent of each other, and cell level equilibria arise from all possible combinations of membrane segment equilibria. In the case of a single membrane segment equilibrium, cell level equilibrium lines intersect once in a single stable equilibrium (panel A, solid line for P_0, dashed line for P_1) and differences between P_0 and P_1 can only arise if the two membranes persistently experience different auxin concentrations or fluxes, thus simply shifting the location of this single equilibrium. By contrast, in the case of a bistable membrane segment, cell level equilibrium lines intersect nine times, producing a total of four stable equilibria: two alternative polar states, an apolar rest state, and a bipolar state (B). If, by contrast, P_0 and P_1 do influence each other via competition for a limiting PIN pool, different situations arise. In the case of a membrane segment with a single equilibrium there is most likely still only one, symmetrical, equilibrium at the single-cell level (A). In the case of a bistable membrane segment model there may be only two stable apolar equilibria (C), or an additional apolar rest state, in which P_0 and P_1 are equal and low (D), but no bipolar state is present.

The authors demonstrated that, in an otherwise homogeneous tissue, persistent sinks attract a small initial flux, causing PINs to orient toward them and auxin patterns to be built up. They showed that, if the degradation of auxin in sinks is sufficiently fast, auxin concentrations become lowest in the sinks, producing with-the-flux and down-the-gradient patterning as expected for with-the-flux models. If, instead, sinks degrade auxin relatively slowly, sinks turn into auxin maxima, resulting in with-the-flux but up-the-gradient PIN localisation. This flexibility is used to simulate, in a 2D tissue, the combination of up-the-gradient maximum formation in the epidermis and with-the-flux down-the-gradient vein formation in the subepidermal tissues, by assuming that primordia act as auxin sinks for the epidermis and as auxin sources for the underlying tissues (see Fig. 1C). In addition, whereas in the epidermis linear feedback resulting in laminar up-the-gradient flows was used, in the subepidermal tissues quadratic feedback was used to generate spatially distinct veins.

Our mathematical analysis of the Stoma et al. (Stoma et al., 2008) model is shown in Box 4. For superlinear, quadratic feedback, we find that a situation with one stable and one unstable equilibrium (see Glossary, Box 1) for membrane segment PIN levels occurs (Fig. 3A). Below the unstable equilibrium, the PIN and auxin levels go to the low stable equilibrium. Above the unstable equilibrium, unlimited growth of PIN and auxin concentrations takes place. This is a special case of bistability, with two separate regions of membrane segment behaviour, but not two stable equilibria. Owing to the absence of a limiting PIN pool, membrane PIN levels are fully independent of each other and only depend on local flux. Consequently, given a bistable membrane segment, a single cell can have four equilibria that are combinations of the two equilibria at each membrane segment. There is a single stable equilibrium in which both membrane segments have the same low PIN level, which we will refer to as the apolar rest state. In addition to this, there are three unstable equilibria, separating regions for which either one or both of the membrane segments obtain unlimited PIN levels. Thus, in this model cells can become polar or apolar depending on their initial auxin and PIN concentrations (Fig. 3B).

When we couple five cells into a cell file flanked by a source and a sink, we observe the expected with-the-flux PIN localisation in the direction of the sink, as in the original paper (Fig. 3C). Furthermore, the strength of the sources and sinks does not influence either the ability to polarise or the strength of polarisation (Fig. 3C, upper two cell files). Finally, for parameter settings in which auxin decay is very slow and hence auxin concentrations are higher in the sinks rather than in the source, we also observed up-the-gradient behaviour (Fig. 3C, bottom cell file). PIN polarity can also be formed and maintained in a ring of cells that only receives a transient perturbation in auxin levels (Fig. 3C). Note that as all cells in the ring pump auxin to their right and receive auxin from

Box 4. Mathematical analysis of the flux-based model of Stoma et al. (Stoma et al., 2008)

Membrane segment level

The auxin equation is given by Eq. 1. The PIN equation for this model depends on the feedback of auxin flux on membrane PIN levels. Flux (F) consists of influx and passive and active efflux over the membrane segment:

$$F = i_{pas} + i_{pin}P - eA\,. \tag{7}$$

Note that we use the same terminology as in the auxin equation (Eq. 1). Since in the cell to which the membrane segment belongs auxin is constant, it is incorporated in i_{pas} and i_{pin}. Feedback of the auxin flux on membrane segment PIN levels is modelled through an increased recycling rate of PINs (k_{on}). Two alternative feedback functions have been proposed by the authors: the linear function $k_{on}=k_{on_b}+k_{on_f}F$ and the quadratic function $k_{on}=k_{on_b}+k_{on_f}F^2$. In both cases, the feedback only takes place when the flux is larger than 0, i.e. when there is net efflux. See Table 2 for parameter definitions and default values. Incorporating the linear feedback function in the *dP/dt* equation (Eq. 3) gives the PIN equilibrium line:

$$P = \begin{cases} \dfrac{k_{on_b} + k_{on_f}\left(i_{pas} - eA\right)}{k_{off} - k_{on_f} i_{pin}} & \text{if } F > 0 \\ \dfrac{k_{on,b}}{k_{off}} & \text{if } F \le 0 \end{cases}, \tag{8}$$

which gives the dashed line in Fig. 3A or 3D. This line can intersect twice with the auxin equilibrium line given by Eq. 2 (but see Fig. 3D). The lower equilibrium is stable and the upper is unstable. Above this equilibrium, unlimited increase of PINs and auxin takes place. The PIN equilibrium line with quadratic feedback gives similar results (dotted line in Fig. 3A).

Single-cell level

At the single-cell level, the authors assume the availability of PINs to be non-limiting. Hence, P_0 and P_1 can be described by Eq. 4b and, assuming that auxin concentrations are in dynamic equilibrium (Eq. 6), PIN equilibrium lines are given by:

$$P_i = \frac{k_{on_f}\left(i_{pas}d - ep\right) + k_{on_b}(e+d)}{k_{off}(e+d) - k_{on_f} i_{pin} d} \text{ with } i = 0,1. \tag{9}$$

Eq. 9 indeed shows that P_0 and P_1 are independent of each other. The equilibrium lines are exactly horizontal and vertical (Fig. 3B, solid lines for P_0 and dashed lines for P_1), intersecting once in a stable apolar equilibrium and three times in unstable equilibria. Above and to the right of these unstable equilibria, unlimited growth of either P_0 or P_1 or both takes place.

Adding a limiting PIN pool

We include a limiting PIN pool by incorporating the feedback functions into Eq. 5 rather than into Eq. 4b. The resulting equilibrium lines have similar shapes for linear and quadratic feedback (Fig. 3G). Owing to the limiting PIN pool, the top part of the PIN equilibrium line curves to the right, allowing for two stable equilibria at the membrane segment level. At the single-cell level, the curves now obtain a complicated shape that allows them to intersect in three stable equilibria: two polar and an apolar rest state (Fig. 3H).

their left neighbour, a circular auxin flux arises that results in a pattern in which final auxin levels are the same across all cells (Fig. 3C). Together, this demonstrates that the model displays polarity-driven self-organisation.

For a small range of parameters, linear feedback also permits two membrane segment equilibria (Fig. 3A), four single-cell equilibria (Fig. 3B) and self-organised polarity-driven patterning (Fig. 3C), as for quadratic feedback. However, for most parameter values, the upper unstable membrane segment equilibrium, and the domain of unlimited PIN levels that it demarcates, do not occur and instead only a single stable equilibrium will be produced (Fig. 3D). Under these conditions, the single-cell level model will have a single stable equilibrium, resulting in apolar cells (Fig. 3E). In the absence of cell polarity, the tissue level pattern now strongly depends on the persistence of sources and sinks and is not able to sustain itself after a temporal perturbation. Hence, the model behaves in a gradient-driven rather than a self-organising manner (Fig. 3F).

We conclude that the Stoma et al. (Stoma et al., 2008) model has the ability to self-organise for both linear and superlinear feedback, although self-organisation occurs in a considerably broader parameter range for the superlinear than the linear feedback. Note that it was analytically shown by Mitchison (Mitchison, 1980) that the formation of distinct veins rather than laminar flows in 2D tissue poses the more stringent requirement for superlinear feedback. This additional requirement for 2D symmetry breaking to generate distinct veins cannot be recovered using our 1D framework.

Altering the model to include a limiting PIN pool

A much discussed aspect of most flux-based models is the low auxin concentrations that they produce in veins (Kramer, 2008; Rolland-Lagan and Prusinkiewicz, 2005), which disagrees with the experimental data (Scarpella et al., 2006). The (non-physiological) cell level assumption of a PIN pool that is so large that membrane segments do not compete for it (termed 'unlimited') can be the cause of low auxin levels in the veins, as it allows for an unlimited increase in membrane PIN levels in response to auxin flux, and hence an unlimited efflux of auxin out of these flux channels.

By incorporating a limiting PIN pool (see Box 4) into the Stoma et al. (Stoma et al., 2008) model, maximum membrane PIN levels become limited by the total amount of PINs that a cell contains. Note that a similar effect can be obtained by assuming a saturating feedback function, which limits the level of PINs that auxin can induce on a membrane segment. At the membrane segment level, the addition of a finite PIN pool causes the model to become truly bistable (Fig. 3G), with a stable high equilibrium as opposed to a region of unlimited growth, independent of whether a linear or quadratic feedback is assumed. In addition, this bistability occurs for much broader parameter regimes.

At the single-cell level, there is still an apolar rest state, in which both membrane segments have the same low PIN concentration, but now there are two polar equilibria in which one membrane segment has a high but limited PIN concentration and the other has a low PIN level (Fig. 3H). The addition of the finite PIN pool abolishes the state in which both membranes can have (infinitely) high PIN levels. The increased parameter region in which membrane bistability occurs together with the abolishment of the bipolar equilibrium induced by the finite PIN pool increase the robustness with which polarity-driven self-organised patterning is generated by the model.

At the tissue level, the model with a limiting PIN pool behaves similarly to the model without a limiting PIN pool (Fig. 3C), the difference being that polar cells now have a low PIN concentration on one membrane segment but a finite, high PIN concentration on the other. Thus, adding a finite PIN pool eliminates the unlimited growth of PIN concentrations and thus limits the maximal flux out of the cells. This is sufficient to allow auxin concentrations to build up in veins, as was demonstrated by Feugier and Iwasa (Feugier and Iwasa, 2006).

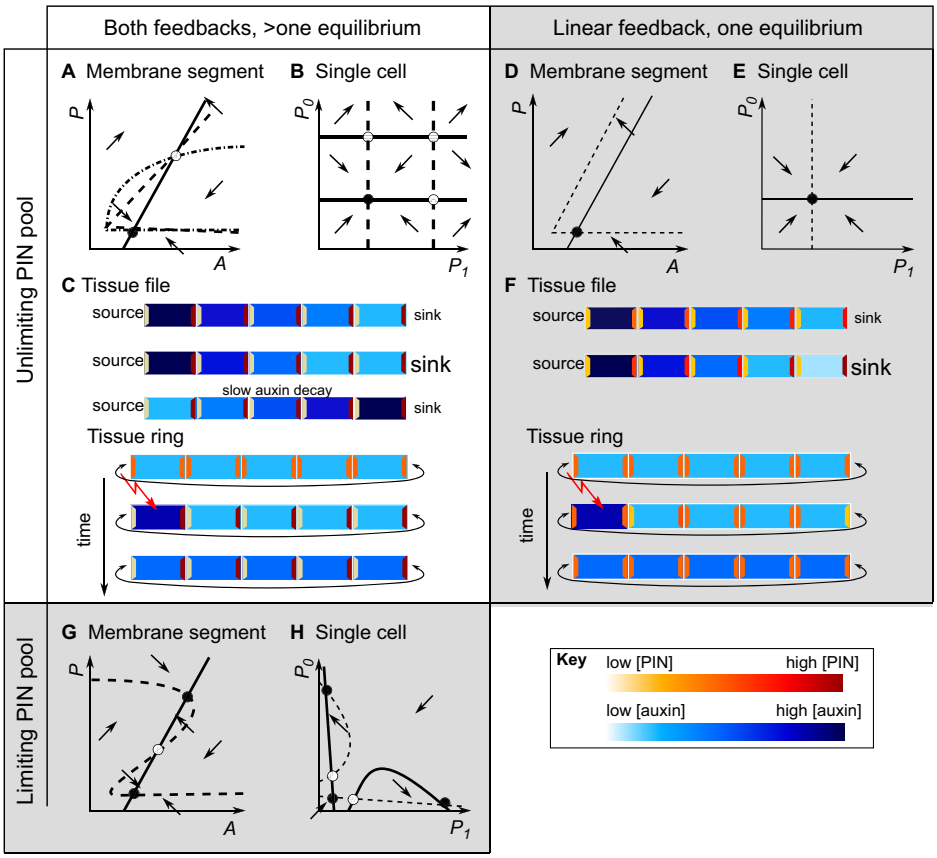

Fig. 3. Analysis of the flux-based model of Stoma et al. (Stoma et al., 2008). Analysis is without (A-F) or with (G,H) a limiting PIN pool. In membrane segment level *A-P* phase planes (A,D,G), solid lines are *A* equilibrium lines and dotted or dashed lines are *P* equilibrium lines. In single-cell P_0-P_1 phase planes (B,E,H), solid lines are P_0 equilibrium lines and dashed lines are P_1 equilibrium lines. Black circles in phase planes represent stable equilibria, whereas white circles indicate unstable equilibria. Arrows indicate the direction of the dynamics of the system variables. (**A**) At the membrane segment level, the PIN equilibrium line resulting from either linear feedback under particular limited parameter settings (dashed line) or from superlinear feedback for all parameter settings (dotted line) intersects twice with the auxin equilibrium line (solid line). (**B**) These two equilibria lead to four equilibria at the single-cell level, one of which is stable. Additionally, there are three regions where either P_0 or P_1 or both increase unlimitedly. (**C**) In a file of cells, the with-the-flux cell polarity is not dependent on the strength of the sink (upper two cell files). For slow auxin degradation, with-the-flux but up-the-gradient polarisation arises (bottom cell file). In a ring of cells, a transient perturbation (red arrow) causes stable polarisation. (**D**) For linear feedback, most parameter settings produce a PIN equilibrium line that allows for only one equilibrium at the membrane segment level. (**E**) This results in a single stable equilibrium at the single-cell level. (**F**) At the tissue level, patterning is now gradient-driven, with cell polarity depending on the strength of the sink at the end of the cell file, and transient perturbation (red arrow) in a ring of cells failing to produce persistent patterning. (**G**) If a limiting PIN pool is assumed, the membrane segments become bistable, both for linear and superlinear feedback. (**H**) At the cell level this results in two stable polar equilibria and a stable apolar rest state. Default parameter settings are used (see Table 2), except: (A) k_{off}=0.1 for both feedbacks; (D) k_{off}=0.5, linear feedback; (G,H) k_{off}=0.5, linear feedback. Note that similar behaviour can be obtained for a range of parameters.

Example 2: concentration-based model

Smith et al. (Smith et al., 2006) formulated a model for phyllotaxis in the growing shoot apical meristem. Membrane PIN levels were assumed to depend positively on the auxin levels in neighbouring cells. The authors used a superlinear saturating feedback function (see Glossary, Box 1), meaning that at first PIN levels increase more than linearly with auxin concentrations until maximum membrane PIN levels are reached. In addition, a limited PIN pool is assumed, causing a competition for PINs between the different membrane segments of a cell. Finally, auxin pumping by the PINs is assumed to saturate with auxin levels in the neighbouring cell. The authors show that, for an initially homogenous ring of cells, evenly spaced peaks of auxin arise after the application of small, transient perturbations, with PINs pointing toward the neighbouring cell with the highest auxin level. In a 2D epidermal tissue layer, the model also produced distinct peaks; however, this occurred at variable distances from one another. However, after incorporating differences in auxin handling between the cell types of different meristem domains, the model can produce stable phyllotaxis patterns. The authors furthermore showed that distinct phyllotaxis patterns can be reproduced by the model depending on parameter values such as meristem size and the transport and diffusion of auxin.

Our analysis of the model by Smith et al. (Smith et al., 2006) is described in Box 5. We find that, at the membrane segment level, the model indeed allows for bistable behaviour (Fig. 4A). Combined with the limiting PIN pool that causes competition for PINs between membrane segments, this results in a cell model with two stable equilibria in which either P_0 is high and P_1 is low or vice versa (Fig. 4B). Hence, cells in this model display polar behaviour. Note that this differs from the model by Stoma et al. (Stoma et al., 2008) after incorporating a finite PIN pool, in which a stable apolar rest equilibrium was also present (Fig. 3H).

Box 5. Mathematical analysis of the concentration-based model of Smith et al. (Smith et al., 2006)

Membrane segment level

To model auxin dynamics, Smith et al. (Smith et al., 2006) take into account production, decay, influx and efflux processes. Auxin production is assumed to be limited by the amount of auxin already present in the cell. Auxin efflux depends in a saturating manner on auxin content in the neighbouring cell, thus both influx and efflux are dependent on auxin in the neighbouring cell (A_i) and auxin in the cell to which the membrane segment of interest belongs (A_c):

$$\frac{dA_i}{dt} = \frac{p}{1+\kappa A_i} - dA_i + i_{pas} + \frac{i_{pin}P_iA_c^2}{h_{pin}^2 + A_i^2} - e_{pas}A_i - \frac{e_{pin}A_i^2}{h_{pin}^2 + A_c^2} \text{ with } i = 0,1, \quad (10)$$

in which κ is the factor by which auxin inhibits its own production, e_{pas} is the passive efflux out of the neighbouring cell and e_{pin} is the PIN-mediated efflux, which is half maximum when $A=h_{pin}$. Note that both A_c and the PINs on the membrane of a neighbouring cell are still assumed to be constant. The resulting auxin equilibrium line is given by:

$$P_i = \frac{h_{pin}^2 + A_i^2}{i_{pin}A_c^2}\left(A_i\left(d + e_{pas}\right) + \frac{e_{pin}A_i^2}{h_{pin}^2 + A_c^2}\right) - \frac{p}{1+\kappa A_i} - i_{pas} \text{ with } i = 0,1. \quad (11)$$

Smith et al. (Smith et al., 2006) assume the PIN pool to be limiting, all PINs to reside on membranes and PIN dynamics to always be in equilibrium. Thus, they determine the PIN equilibrium line directly:

$$P = \frac{P_{tot}b^A}{\sum_n b^{A_i}}, \quad (12)$$

where b is a base parameter that the authors set to 2 or 3, and the sum is taken over the auxin concentrations in all neighbouring cells (n). P_{tot} contains explicit (auxin-induced) production and decay of PINs. Given that we maximally consider two auxin concentrations in neighbouring cells, we can replace Eq. 12 with:

$$P_i = \frac{P_{tot}b^{A_i}}{b^{A_i} + b^{A_j}} \text{ with } i = 0,1 \text{ and } j = 1,0. \quad (13)$$

Note that, at the membrane segment level, we assume A_j to be constant. There are a total of three intersection points between the PIN and auxin equilibrium lines (dashed and solid lines in Fig. 4A), of which the outer two equilibria, corresponding to low and high PIN levels, are stable.

The PIN equilibrium line shifts with the value of b^{A_j} (Eq. 13). It moves to the right when A_j is high and to the left when A_j is low (Fig. 4D,E, respectively), potentially eliminating two equilibria and thus the potential for bistability. Thus, whether cells can polarise depends on their local auxin context.

Single cell

For the cell level, the PIN equilibrium line is given by Eq. 13, in which now both A_i and A_j are variable. We substitute these in the auxin equations (Eq. 10) and solve to obtain the auxin equilibrium lines in Fig. 4B. These intersect three times in two stable polar equilibria separated by an unstable one. Since the PINs are assumed to be in equilibrium with the auxin levels (Eq. 13), they can be directly deduced from the auxin levels in the equilibria.

Removing the limiting PIN pool

To study how the model behaviour changes if there is no competition for a limited PIN pool, we have to reverse-engineer Eq. 12. The PIN equation is given by Eq. 5 and there are two possible ways to create the sigmoid PIN equilibrium line through feedback of auxin on k_{on}: through a non-saturating ($k_{on}=k_{on_b}+k_{on_f}\,b^A$) or a saturating [$k_{on}=k_{on_b}+k_{on_f}\,b^A/(b^{h_A}+b^A)$] function. Substituting these feedbacks into the PIN equation without a limiting PIN pool (Eq. 3) results in the PIN equilibrium lines:

$$P = \frac{1}{k_{off}}\left(k_{on_b} + k_{on_f}b^A\right), \quad (14a)$$

$$P = \frac{1}{k_{off}}\left(k_{on_b} + \frac{k_{on_f}b^A}{b^{h_A} + b^A}\right). \quad (14b)$$

Both of these lines can intersect more than once with the auxin equilibrium line. In the case of Eq. 14a there are two equilibria (Fig. 4F). The lower one is stable, and the upper, which is unstable, separates a region of unlimited increase in PINs. In the case of Eq. 14b, the system has two stable equilibria separated by an unstable one (Fig. 4H). At the cell level this results in one stable equilibrium and three regions of increase of either P_0, P_1, or both for Eq. 14a (Fig. 4G) or four stable equilibria, two polar and two apolar, for Eq. 14b (Fig. 4I).

In a file of cells, we find that PINs are oriented up-the-gradient (Fig. 4C), which is consistent with the premise of the model whereby PINs are localised on the membrane segment apposing the neighbouring cell with highest auxin levels. Polarised cells display a low PIN concentration on the membrane segment facing the sink and a high PIN concentration on the membrane facing the source, and these levels are independent of the strength of the source and sink. When a ring of cells is simulated, a transient perturbation in one of the cells spreads throughout the entire cell file, producing a persistent polarisation of all cells. The cell that received the perturbation, in the form of a transient increase in auxin, develops into an auxin maximum due to the pointing of the polarised cells towards it, and an auxin minimum arises at the opposing side of the cell file, from which the polarised cells point away. Thus, in contrast to what happens in the flux-based model, the polarisation of cells is accompanied here by a patterned rather than homogeneous auxin distribution (Fig. 4C). Our analysis thus confirms that pattern formation in the Smith et al. (Smith et al., 2006) model is self-organising, and that this self-organisation is polarity-driven, in agreement with the model behaviour reported in the original paper.

The feedback function used by Smith et al. (Smith et al., 2006) results in a PIN equilibrium line (see Glossary, Box 1) that shifts as a function of the difference in auxin concentration between two neighbouring cells (see Fig. 4D,E). As a result, one of the two membrane segment equilibria may disappear, abolishing membrane bistability and cell polarity. Therefore, not all cells within a tissue necessarily experience the auxin concentration differences that are necessary to polarise. This might explain why the authors observed strongly polarised cells close to maxima, but weaker or no polarisation at a greater distance from the maxima.

Removing the limiting PIN pool from the model

Next we examine whether the model behaviour changes if we assume that there is no competition between membrane segments for a limiting PIN pool (see Box 5 for details). Obviously, this is not increasing the physiological realism of the model. However, performing this analysis allows us to compare the flux-based and concentration-based models both under conditions with and without a finite PIN pool. On the membrane segment level, we find that there is still bistability, with either two stable and one unstable equilibrium as in Fig. 4A (Fig. 4H, for saturating feedback) or with one stable and one unstable equilibrium (Fig. 4F, for non-saturating feedback).

On the cell level, we find four alternative equilibria for non-saturating feedback (Fig. 4G), which result from combining the two

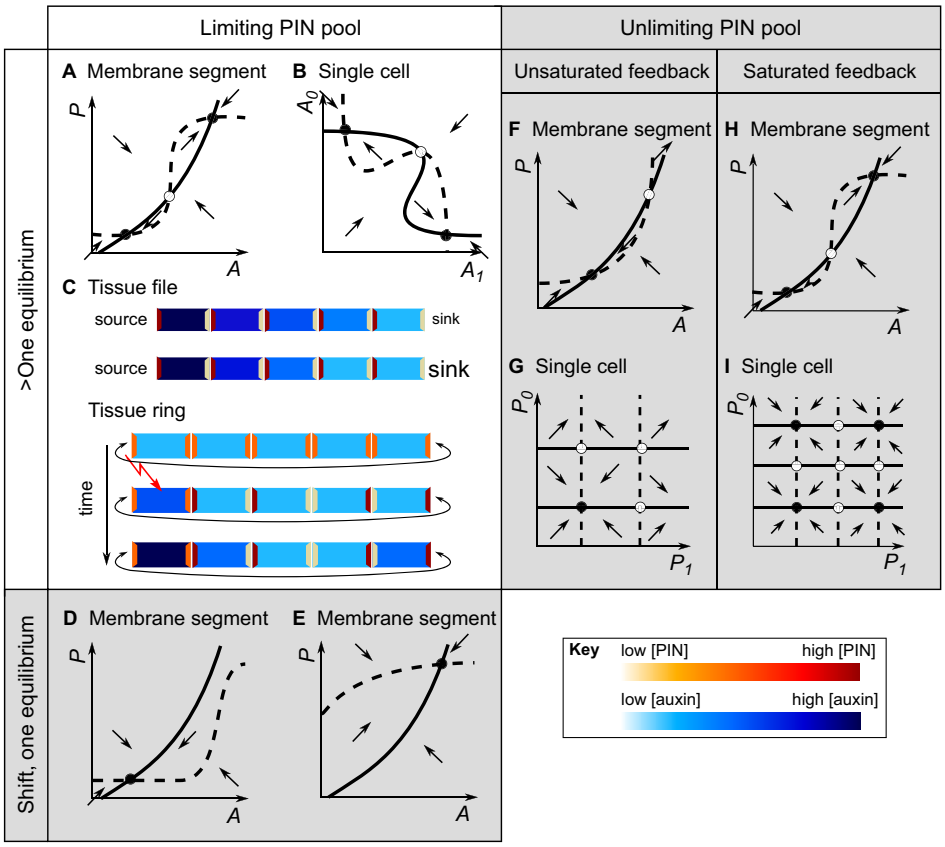

Fig. 4. Analysis of the concentration-based model of Smith et al. (Smith et al., 2006). Analysis is with (A-E) and without (F-I) a limiting PIN pool. Equilibrium lines, equilibria and arrows are the same as in Fig. 3 for the membrane segment *A-P* (A,D,E,F,H) and single-cell (B,G,I) phase planes. In the single-cell A_0-A_1 phase planes (B,G,I), the solid equilibrium line is for A_0 and the dashed equilibrium line is for A_1. (**A**) At the membrane segment level the PIN and auxin equilibrium lines can intersect three times. (**B**) At the single-cell level, there are two stable, polar equilibria. (**C**) At the tissue level, up-the-gradient polarisation occurs with cellular polarity that is independent of the strength of the sink and that can sustain itself in a ring of cells after a transient perturbation (red arrow). (**D**,**E**) When A_j is high (D) or low (E), the PIN equilibrium line moves such that membrane segment equilibria are lost. (**F**) At the membrane segment level, in the case of non-saturated feedback and a non-limiting PIN pool (Eq. 14a) the PIN equilibrium line can intersect twice with the auxin equilibrium line. (**G**) At the cell level, this results in one stable equilibrium and three unstable equilibria demarcating alternative regions of behaviour in which either one, the other, or both PIN levels increase infinitely. (**H**,**I**) If, instead, a saturated feedback is assumed (Eq. 14b), there are two stable equilibria at the membrane segment level (H) and four stable equilibria, two of which are polar and two apolar, at the cell level (I). Default parameters are used (see Table 2), except: κ=1, h_{pin}=1, b=2, A_c=12; (A) A_j=10, dynamic PINs (Eq. 14b): k_{onb}=0.01, k_{onf}=5, k_{off}=0.5 for both feedbacks; (D) A_j=20; (E) A_j=1; (F) dynamic PINs (Eq. 14a): k_{onb}=0.01, k_{onf}=0.5, k_{off}=5. Note that similar behaviour can be obtained for a range of parameters.

equilibria for P_0 with the two equilibria for P_1. The single stable equilibrium corresponds to the apolar cell state in which both membrane segments have a low PIN level. The unstable equilibria separate this apolar rest state from the alternative states in which unlimited growth of PINs on either one or both of the membrane segments occurs. If, instead, the feedback is saturating, there are a total of nine equilibria at the single-cell level (Fig. 4H), which result from combining the three equilibria at the membrane segment level. In this case there are four stable equilibria: one apolar, two alternative polar equilibria, and one bipolar. Thus, despite the removal of the PIN pool the model retains its potential to produce polar cells. However, it acquires a bipolar state, with high PINs on both membranes or a region in which both membranes increase their PIN level unlimitedly, and an apolar rest state in which both membranes have low PIN levels. Consequently, the robustness of polarity-driven self-organised patterning is decreased. Thus, the tissue level behaviour is similar upon removal of the PIN pool, but whether a cell is polar or not now depends more strongly on its context.

Evaluation of other PAT models

Having analysed these two example models in detail, we now briefly discuss our analysis of other PAT models found in the literature. The full analysis can be found in supplementary material Appendix S1, and an overview of all model assumptions and the generated behaviour is given in Table 2.

Flux-based models

In addition to the model by Stoma et al. (Stoma et al., 2008) that we used as an example, we analysed a variety of published flux-based models (Mitchison, 1980; Mitchison, 1981; Feugier and Iwasa, 2006; Feugier et al., 2005; Fujita and Mochizuki, 2006; Alim and Frey, 2010). Summarising, we find that all flux-based models, independent of the shape of the feedback function, auxin pumping dynamics or whether a limiting PIN pool is assumed, are capable of generating polarity-driven self-organised auxin and PIN patterns. Furthermore, all these models contain a stable rest state equilibrium at the single-cell level, in which both membranes contain low PIN levels, that is separated from the two alternative

polar states by unstable equilibria. Consequently, cell polarisation in these models requires perturbations that push the system beyond these unstable equilibria into the realm of the polar equilibria.

We find that in those models (Feugier and Iwasa, 2006; Feugier et al., 2005; Fujita and Mochizuki, 2006; Alim and Frey, 2010), in which a finite PIN pool is assumed, no bipolar equilibrium with high PIN levels at both membranes is present. By contrast, in the early models by Mitchison (Mitchison, 1980; Mitchison, 1981) and in the model by Stoma et al. (Stoma et al., 2008) (which is based on these early models) no limiting PIN pool is incorporated and a bipolar state does occur, resulting in more possibilities for nonpolar cells. Similar to the model by Stoma et al. (Stoma et al., 2008), the other flux-based models show with-the-flux behaviour, but can generate up-the-gradient auxin transport depending on the strength of localised sinks. In all cases, we find that a superlinear dependence of membrane PIN levels on auxin flux increases the parameter range for membrane bistability and hence the robustness of self-organised patterning.

Concentration-based models

Besides the model by Smith et al. (Smith et al., 2006), we applied our analysis to several further published concentration-based models (Jönsson et al., 2006; Merks et al., 2007; Newell et al., 2007; Sahlin et al., 2009). For the model by Newell et al. (Newell et al., 2007), which combines auxin concentration feedback on PINs and mechanical effects, we have not considered the mechanical effects. Concentration-based models do not automatically allow for self-organised patterning. For polarity-driven self-organised patterning to arise, either a non-linear feedback function (Smith et al., 2006; Jönsson et al., 2006) and/or non-linearity in auxin pumping dynamics (Jönsson et al., 2006; Merks et al., 2007; Sahlin et al., 2009) is necessary. This difference between concentration-based and flux-based models is due to the inherent presence of non-linearity in flux-based models. First, in most flux models, feedback only occurs for net efflux, with PIN levels abruptly switching to the minimum concentration for negative efflux. Hence, even a seemingly linear function is transformed into a non-linear function. Second, flux is essentially the product of the PIN level and auxin concentration. Thus, even if flux feeds back linearly on PINs, this results in a direct positive feedback of PINs on PINs, effectively making the feedback non-linear. Increased non-linearity in feedback or auxin pumping, saturating feedback and a finite PIN pool contribute to the robustness of polarity-driven self-organised patterning, as was the case in flux-based models. Introduction of a limiting PIN pool in concentration-based models abolishes both the bipolar and the apolar rest equilibrium, whereas in flux-based models only the bipolar equilibrium disappears. Consequently, concentration-based models incorporating a finite PIN pool always produce polar cells without requiring any substantial perturbation, as no stable apolar cell state is present.

In addition to polarity-driven self-organised patterning, we find an additional self-organisation mechanism in concentration-based models that occurs if a finite PIN pool is combined with a linear feedback function and linear auxin pumping dynamics (Newell et al., 2007; Jönsson et al., 2006). Owing to the absence of non-linearity, no polarity-driven self-organisation can arise. However, on the tissue level, auxin and PIN polarity patterns look similar, as for the polarity-driven self-organisation discussed for Smith et al. (Smith et al., 2006). The principal difference is that, in isolation, single membrane segments are not bistable and single cells are not polar, and hence polarity arises only at the tissue level. This mechanism of self-organisation resembles Turing-type patterning. The positive feedback from cellular auxin levels on PIN levels in the membranes of neighbouring cells amplifies local auxin maxima, thus functioning as short-range activation, while the resulting depletion of auxin from surrounding tissue prevents the formation of nearby maxima, thus serving as long-range inhibition. For certain parameter conditions, and combined with a finite PIN pool that causes competition for PINs between membranes and hence promotes cellular polarity, these effects destabilise the single stable equilibrium of the system and lead to the formation of auxin maxima and PIN polarity (see our bifurcation analysis in supplementary material Appendix S1). The detailed analysis by Sahlin et al. (Sahlin et al., 2009) suggests that this mechanism might, in addition to the isolated maxima needed for phyllotactic patterns, also generate stripe-like patterns.

Finally, in contrast to flux-based models, concentration-based models are capable only of generating up-the-gradient patterning.

Mechanistic models

An alternative hypothesis for PIN polarisation was introduced by Heisler et al. (Heisler et al., 2010). The model was inspired by the observation that PIN polarity is correlated with the alignment of cortical microtubules. This led the authors to propose that PINs localise to membrane segments adjoining cell walls that experience the most stress, which in turn is the result of local cell expansion due to auxin. The model can thus be seen as a more mechanistic version of concentration-based models, with wall stress being the readout of auxin content in the neighbouring cells. The combination of non-linear auxin pumping dynamics and a finite PIN pool causes the model to behave in a self-organised polarity-driven manner that generates up-the-gradient patterning, similar to concentration-based models.

Recently, Wabnik et al. (Wabnik et al., 2011) proposed yet another alternative hypothesis for the feedback of auxin on membrane PIN levels. In their model, extracellular auxin binds to free receptors in the apoplast. The resulting auxin-receptor complexes inhibit endocytosis of PIN proteins on the nearest membrane segment. Furthermore, the complexes limit the diffusion of auxin and receptor, producing both an intra-apoplast auxin gradient and competition for receptors between segments on either side of the cell wall. We extended our framework with cell wall compartments and receptor variables in order to study this model (see supplementary material Appendix S1). Our analysis shows that the model allows for membrane bistability and cell polarity and produces with-the-flux tissue polarisation patterns under the additional requirement that auxin has a low diffusion speed in the cell wall, hence allowing for wall gradients.

Models for fountain-like patterns

For the model by Stoma et al. (Stoma et al., 2008), we discussed how the authors used the flux-based mechanism to generate both up-the-gradient maximum formation in the epidermis and down-the-gradient with-the-flux vein formation in subepidermal tissues. In order to achieve this, distinct model settings were required for the different tissue layers. Similarly, Merks et al. (Merks et al., 2007) proposed a concentration-based model to simulate these two processes in combination. In addition to the assumption that cells position their PINs toward the neighbouring cell with the highest auxin concentration, auxin is assumed to induce PIN expression (Vieten et al., 2005), which destabilises the position of the auxin maximum. As a result, the initially epidermal maximum propagates

Table 2. Evaluation of different models according to assumptions and behaviour on all levels of organisation

Reference	Mechanism	Feedback function	Biological interpretation	Auxin transport	Biological interpretation	PIN dynamics	Biological interpretation	Bistable membranes?	Polar cells?	Maximal organisation	Up or down gradient?
Stoma et al., 2008	Flux-based	$k_{on} \propto F$	Exocytosis increases linearly with flux	Linear: $T \propto PA$	Neither [PIN] nor [auxin] is limiting	$\frac{dP}{dt} = k_{on} - k_{off}P$	PINs cycle to and from the membrane; exocytosis does not lower the availability of cytosolic PINs	Yes	Yes	Self-organised: polarity-driven	Up and down
		$k_{on} \propto F^2$	Exocytosis increases more with flux when flux becomes higher								
Smith et al., 2006	[]-based	$P \propto \frac{b^A}{\sum_n b^{A_n}}$	[PIN] increases faster with higher [auxin] in neighbour, and saturates for high [auxin]	Saturated: $T \propto P\frac{A^2}{h^2 + A^2}$	[PIN] is limiting: transport saturates for high [auxin] in neighbouring cell	$P \propto \frac{P_c b^A}{\sum_n b^{A_n}}$ PINs produced and decayed in P_c	PIN pool is limiting, all PINs are on the membrane, and cycling is in equilibrium; auxin induces PIN expression	Yes	Yes	Self-organised: polarity-driven	Up
Mitchison, 1980	Flux-based	$D \propto \frac{F^2}{h^2 + F^2}$	Permeability increases more with flux when flux becomes higher and saturates for high flux	Linear: $T \propto PA$	Neither permeability nor [auxin] is limiting	–	–	Yes	Yes	Self-organised: polarity-driven	Down
Mitchison, 1981	Flux-based	$D \propto F^2$	Permeability increases more with flux when flux becomes higher	Linear: $T \propto PA$	Neither permeability nor [auxin] is limiting	–	–	Yes	Yes	Self-organised: polarity-driven	Down
Feugier et al., 2005	Flux-based	Various	Various	Various	Various	Various	Various	Yes	Yes	Self-organised: polarity-driven	Down
Feugier and Iwasa, 2006	Flux-based	$k_{on} \propto F^2$	Exocytosis increases more with flux when flux becomes higher	Linear: $T \propto PA$	Neither [PIN] nor [auxin] is limiting	$\frac{dP}{dt} = k_{on}P_{tot} - k_{off}P$	PINs cycle to and from the membrane, PIN pool is limiting	Yes	Yes	Self-organised: polarity-driven	Down
Fujita and Mochizuki, 2006	Flux-based	$P \propto \frac{1}{1 + e^{-F}}$	[PIN] increases more with flux when flux becomes higher	Linear: $T \propto PA$	Neither [PIN] nor [auxin] is limiting	$P \propto \frac{1}{1 + e^{-F}}$	PIN pool is limiting, all PINs are on the membrane and cycling is in dynamic equilibrium	Yes	Yes	Self-organised: polarity-driven	Down
Alim and Frey, 2010	Flux-based	$k_{on} \propto F^2$	Exocytosis increases more with flux when flux becomes higher	Linear: $T \propto PA$	Neither [PIN] nor [auxin] is limiting	$\frac{dP}{dt} = k_{on}P_{tot} - k_{off}P$	PINs cycle to and from the membrane, the PIN pool is limiting	Yes	Yes	Self-organised: polarity-driven	Down
Jönsson et al., 2006	[]-based	$P \propto \frac{A}{\sum_n A_n}$	[PIN] increases linearly with [auxin] in neighbour and saturates for high [auxin]	Linear: $T \propto PA$	Neither [PIN] nor [auxin] is limiting	$P \propto \frac{P_{tot}A}{\sum_n A_n}$	PIN pool is limiting, all PINs are on the membrane, cycling is in equilibrium	No	No	Self-organised: other (see text)	Up
		$k_{on} \propto \frac{A^3}{h^3 + A^3}$	Exocytosis increases faster with higher [auxin] in neighbour and saturates for high [auxin]	Saturated: $T \propto P\frac{A}{h + A}$	[PIN] is limiting: transport saturates for high [auxin]	$\frac{dP}{dt} = k_{on}P_{tot} - k_{off}P$	PINs cycle to and from the membrane, PIN pool is limiting	Yes	Yes	Self-organised: polarity-driven	Up
Merks et al., 2007	[]-based	$k_{on} \propto \frac{A}{h + A}$	Exocytosis increases linearly with [auxin] in neighbour and saturates for high [auxin]	Saturated: $T \propto P\frac{A}{h + A}$	[PIN] is limiting: transport saturates for high [auxin]	$\frac{dP}{dt} = k_{on}P_c - k_{off}P$ PINs produced and decayed in P_c	PINs are produced, decayed and cycle to and from the membrane; auxin induces PIN expression	Yes	Yes	Self-organised: polarity-driven	Up
Newell et al., 2007	[]-based	$k_{on} \propto A$	Exocytosis increases linearly with [auxin]	Linear: $T \propto PA$	Neither [PIN] nor [auxin] is limiting	$\frac{dP}{dt} = k_{on}P_{tot} - k_{off}P$	PINs cycle to and from the membrane, the PIN pool is limiting	No	No	Self-organised: other (see text)	Up
Sahlin et al., 2009	[]-based	Various	Various	Saturated: $T \propto P\frac{A}{h + A}$	[PIN] is limiting: transport saturates for high [auxin]	$\frac{dP}{dt} = k_{on}P_{tot} - k_{off}P$	PINs cycle to and from the membrane, the PIN pool is limiting (some tests performed with an unlimited PIN pool)	Yes	Yes	Self-organised: polarity-driven	Up

Table 2 continued on next page.

Table 2. Continued

Bayer et al., 2009	Flux-based and []-based	$P \propto \frac{b^F}{\sum_n b^{F_n}}$ $P \propto \frac{b^A}{\sum_n b^{A_n}}$	[PIN] increases faster with higher flux/[auxin] in neighbour and saturates for high flux/[auxin]	Saturated: $T \propto P\frac{A^2}{h^2+A^2}$	[PIN] is limiting: transport saturates for high [auxin]	$P \propto \frac{P_c b^F}{\sum_n b^{F_n}}$ $P \propto \frac{P_c b^A}{\sum_n b^{A_n}}$ PINs produced and decayed in P_c	PINs are produced, decayed; cycling is in dynamic equilibrium and all PINs are on the membrane; auxin induces PIN expression	Yes	Yes	Self-organised: polarity-driven	Up and down
Heisler and Jönsson, 2006	[]-based	$P \propto \frac{A}{\sum_n A_n}$	Exocytosis increases linearly with [auxin] in neighbour and saturates for high [auxin]	Saturated: $T \propto P\frac{A}{h+A}$	[PIN] is limiting: transport saturates for high [auxin]	$P \propto \frac{P_{tot} A}{\sum_n A_n}$	PIN pool is limiting, all PINs are on the membrane, and cycling is in dynamic equilibrium	Yes	Yes	Self-organised: polarity-driven	Up
Wabnik et al., 2011	Cell wall []-based	$k_{off} \propto \frac{1}{h+A}$	Endocytosis decreases linearly with [auxin] in cell wall and saturates for high [auxin]	Saturated: $T \propto P\frac{A}{h+A}$	[PIN] is limiting: transport saturates for high [auxin]	$\frac{dP}{dt} = k_{on}P_c - k_{off}P$ PINs produced and decayed in P_c	PINs are produced, decayed and cycle to and from the membrane; auxin induces PIN expression	Yes	Yes	Self-organised: polarity-driven	Up

[] is used for concentration, *D* represent membrane permeability, *T* represents transport.

subepidermally through the tissue and leaves basally pointing PINs in its wake. Thus, whereas the model by Stoma et al. (Stoma et al., 2008) required different assumptions for different tissue layers to combine auxin maximum and vein formation, the model by Merks et al. (Merks et al., 2007) is only capable of generating the two patterns sequentially, with one replacing the other.

In another attempt to explain fountain-like pattern formation, Bayer et al. (Bayer et al., 2009) developed a model that explicitly combines concentration-based and flux-based feedback, using an auxin level threshold to decide which type of feedback should be applied locally. The model generates auxin maxima in the epidermis by invoking up-the-gradient feedback and then switches to with-the-flux feedback that positions PINs in underlying tissues away from the maximum. In the up-the-gradient regime, the authors chose the same feedback function as in their previous concentration-based model (Smith et al., 2006). Hence, the membrane segments are bistable and single cells are polar, allowing polarity-driven self-organised pattern formation. In the with-the-flux regime, the feedback function is superlinear. As shown by Feugier et al. (Feugier et al., 2005) and following from our analysis, these conditions also allow for polar cells and polarity-driven self-organising vein formation with high auxin concentrations in the veins. However, given that two distinct feedback mechanisms need to be invoked, the overall pattern is not fully self-organised.

Extrapolating our analysis to 2D and 3D tissue and *in vivo* plant patterns

Our analysis is restricted to the self-organising potential of published models at the membrane segment, single-cell and 1D tissue level and the type (orientation) of 1D patterns that they generate. The reason for this restriction is mainly the feasibility of a rigid analytical approach. Obviously, this limits the degree to which we can predict the 2D and 3D tissue patterns generated by the models and how far these model patterns correspond to *in vivo* patterns. For example, based on our analysis we cannot predict the precise spacing and arrangement between phyllotactic maxima or leaf veins. Indeed, Mitchison (Mitchison, 1980) showed analytically that to obtain an additional symmetry breaking in 2D tissue and generate distinct veins rather than laminar flow patterns, superlinear feedback of auxin flux on PIN polarisation is required. Based on our 1D analysis, we can only conclude that both linear and superlinear feedback generate self-organised with-the-flux oriented polarisation patterns, but cannot determine this additional demand for distinct veins. In other words, we can determine the necessary requirements for self-organised patterning, but we cannot determine requirements for a specific phyllotactic or venation pattern. However, we are able to extrapolate our 1D analysis to higher dimensional tissue patterns to a qualitative extent, focusing on the orientation and self-organised nature of the patterning.

Let us consider the fountain and reverse-fountain types of flux pattern observed in the shoot primordia and root tip (Fig. 1C,D). Two main transport directions can be distinguished in both organs: toward (labelled 2) and away (labelled 1) from a maximum. In the root tip (Fig. 1D), auxin flux is directed toward the root tip maximum in the inner tissue layers and away from the maximum in the outer layer(s). The pattern in a shoot primordium is reversed (Fig. 1C). Our 1D analysis reveals how, in each model, PINs can polarise with respect to a maximum. We found that concentration-based models always direct PINs toward an auxin maximum, whereas flux-based models generally locate PINs away from the maximum but can be made to display an opposite orientation under particular parameter conditions. Hence, concentration-based models can explain the arrows labelled 2 in Fig. 1C,D, which point towards the auxin maximum, but cannot explain those labelled 1 in an autonomous manner. However, it has been shown that expression of the gene *PINOID* can switch the polar orientation of PINs from a basal to an apical orientation (Friml et al., 2004) by influencing intracellular PIN trafficking (Michniewicz et al., 2007). Thus, in the root, PINOID expression in the outer tissue layer(s) could account for the switch to away-from-maximum localisation in these layers. However, this would not explain the away-from-maximum arrows in the inner tissues of the shoot primordium. Flux-based models can in theory account for both arrows. However, this requires that the auxin maximum serves as a sink (that attracts auxin) for the inner layers and as a source for the outer layers in the root tip (with the reverse for the shoot primordium) [see model by Stoma et al. (Stoma et al., 2008)].

Thus, based on our analysis we conclude that, despite their ability to generate self-organised patterns, neither concentration-

based nor flux-based models can explain fountain-type patterns in a fully autonomous self-organised manner, but require additional tissue- or location-specific assumptions. This implies either that auxin patterning in plants is not fully self-organised and that tissue-specific responses are required, or that the currently proposed feedback mechanisms need to be revised to fully explain self-organised auxin patterning.

Conclusions

Auxin patterning plays a central role in robust, yet developmentally and environmentally flexible, plant development. The long-standing idea that auxin influences its own transport, thus potentially allowing for self-organised patterning, has inspired numerous modelling studies. Apart from the major and easily understood distinction assumed in the feedback mechanism – whether auxin flux across the membrane or auxin levels in neighbouring cells impacts membrane PIN levels – models differ in their mathematical descriptions of the details of this feedback, as well as of auxin transport dynamics and PIN cycling dynamics. The relevance of these variations for model output is less obvious. In addition, little attention has been devoted to whether the generated model patterns arise in an autonomous self-organised manner or are strongly dependent on persistent prepatterns or additional assumptions. However, largely self-organised patterning is essential for robust, repeated and flexible patterning during plant development. Here we developed a generalised analytical and simulation framework to compare most of the currently published PAT models, translating the wide range of mathematical functions employed into a limited set of underlying biological assumptions, and reporting the model behaviour that this results in on the membrane segment, cell and tissue levels. We focused on the directionality of PIN polarisation and the extent of self-organised patterning that the models generate.

To summarise our analysis, flux-based models are somewhat more flexible in the direction of polarisation that they can generate, and do not necessarily require non-linearity or a limiting PIN pool to generate self-organised patterning. By contrast, concentration-based models allow for two different modes of self-organised patterning, and require less perturbation for cell polarisation to occur in the case of a limiting PIN pool. Still, both model types require largely similar biological assumptions to generate patterns in a robust self-organising manner, and both display only a single strongly preferred direction of polarisation. However, in plants, opposite polarities often co-occur. In the shoot and lateral root primordia, leaves, the primary root and the developing embryo, (reverse) fountain-like patterns are found, with neighbouring cell files displaying opposite PIN polarisations with respect to the same tissue gradient. Based on our analysis, we therefore hypothesise that neither concentration-based nor flux-based models are currently capable of explaining bidirectional fountain-type patterns in a fully self-organised manner.

Future directions

In this exploration of published PAT models, we have demonstrated that all current models explain *in planta* auxin and PIN patterning to the same limited extent and for similar conditions. Consequently, based on our current knowledge it remains unclear which feedback mechanism is at work in real plants – concentration-based, feedback-based, a combination of the two, or an alternative mechanism. Further, it is not clear how these models can explain the robust and repeated formation of fountain-type patterns in primordia and apical and basal meristems. In which directions should future modelling and experimental research proceed in order to answer these questions?

Let us first focus on the modelling. Our analysis shows that a positive auxin-PIN feedback, combined with a non-linearity in either feedback or auxin pumping or a limiting PIN pool, suffices for generating robust self-organised patterning. Thus, we would argue that further extending the number of flux-based and concentration-based models (by varying the type of mathematical functions used for describing the biological processes and by varying how the required non-linearity is incorporated) will not advance the current situation, but will simply provide more of the same results. However, this knowledge does allow us to easily generate alternative feedback models – for example, a feedback of local, intracellular auxin concentration on membrane PIN levels as suggested by Kramer (Kramer, 2009) – that have self-organising capacity, and to study to what extent such alternative feedback models are capable of generating fountain-type patterns in a self-organised manner.

Second, we discussed how tissue-specific PINOID expression combined with a concentration-based feedback, or a differential source and sink behaviour of an auxin maximum for different tissue layers combined with a flux-based model (Stoma et al., 2008), may be capable of generating at least certain fountain-type patterns. However, as these tissue-specific properties are superimposed, this patterning is not fully self-organised. Although only partly successful in the model by Merks et al. (Merks et al., 2007), a possibly fruitful approach might be to incorporate gene expression regulation into PAT models in such a manner that the tissue-specific requirements for different flux orientations are automatically generated as part of the patterning process. Important candidate genes to consider are the PINs themselves, additional exporters such as the P-GLYCOPROTEINs (PGPs), but also auxin importers such as the AUX/LAX genes, and PIN cycling dynamics regulators such as *PINOID* (e.g. Swarup et al., 2000; Bandyopadhyay et al., 2007; Benjamins et al., 2001). Together, these two approaches will hopefully allow us to determine the type of feedback, non-linearities and gene regulation mechanisms that are theoretically capable of generating self-organised fountain patterns.

To establish the mechanisms at work in real plants a combined experimental and modelling approach is necessary. Thus, a third important direction for future research is to formulate more molecularly mechanistic PAT models that allow for explicit experimental verification. This applies to tissue properties, such as cell walls and subcellular compartments, that have been ignored in a subset of the current models, but most importantly to the mechanism by which auxin feeds back on PIN localisation. The field has recently begun to move in this direction with models (Heisler et al., 2010; Wabnik et al., 2010) in which cells measure wall stress or use the ABP1 receptor to sense apoplast auxin levels, rather than measuring auxin levels in neighbouring cells. Although most molecular mechanisms behind the interactions proposed by Heisler et al. (Heisler et al., 2010) have yet to be determined, a property such as wall stress is compliant to experimental manipulation. Similarly, a local requirement for the ABP1 receptor, which plays a central role in the model by Wabnik et al. (Wabnik et al., 2010), can be tested experimentally. In addition, this model requires and predicts a steep auxin gradient in the apoplast. Ideally, spatiotemporally refined methods for measuring extracellular auxin concentrations should be established to test the existence of this gradient. One could also propose more mechanistic models for flux-based feedback, for example by assuming that PINs measure

the auxin efflux that occurs through them, rather than membranes measuring the total net efflux across them, which would be more amenable to experimental tests.

To enable the construction and refinement of these more mechanistic models, we need to gain a much better understanding of PIN cycling, expression and degradation, and how these might depend on auxin levels or fluxes. For example, our analysis points to the importance of a limiting cellular PIN pool for the robustness of self-organised patterning and for realistic auxin levels in veins. However, we also find that, in models that take PIN production and decay into account, the seemingly reasonable assumption that PIN degradation is limited to non-membrane-bound PINs implicitly causes the PIN pool to be non-limiting (Merks et al., 2007; Wabnik et al., 2010). Thus, we need to experimentally verify whether membranes compete for a finite cellular PIN pool by performing detailed quantification of the amount of PIN proteins present in different cellular compartments under different conditions. In addition, for these conditions, experiments using photo-convertible tags should be performed to determine PIN cycling rates to and from the membrane.

The proposed combining of, and iteration between, increasingly mechanistic PAT models and experiments, together with an extension of PAT models to encompass alternative feedback mechanisms and regulated gene expression, will allow us to eventually pinpoint the inner workings of auxin patterning in plants.

Funding
K.v.B. and B.S. are funded by the European Research Council (ERC) Advanced Research Grant 'SysArc'.

Competing interests statement
The authors declare no competing financial interests.

Supplementary material
Supplementary material available online at
http://dev.biologists.org/lookup/suppl/doi:10.1242/dev.079111/-/DC1

References

Alim, K. and Frey, E. (2010). Quantitative predictions on auxin-induced polar distribution of PIN proteins during vein formation in leaves. *Eur. Phys. J. E* **33**, 165-173.
Bandyopadhyay, A., Blakeslee, J. J., Lee, O. R., Mravec, J., Sauer, M., Titapiwatanakun, B., Makam, S. N., Bouchard, R., Geisler, M., Martinoia, E. et al. (2007). Interactions of PIN and PGP auxin transport mechanisms. *Biochem. Soc. Trans.* **35**, 137-141.
Bayer, E. M., Smith, R. S., Mandel, T., Nakayama, N., Sauer, M., Prusinkiewicz, P. and Kuhlemeier, C. (2009). Integration of transport-based models for phyllotaxis and midvein formation. *Genes Dev.* **23**, 373-384.
Benjamins, R., Quint, A., Weijers, D., Hooykaas, P. and Offringa, R. (2001). The PINOID protein kinase regulates organ development in Arabidopsis by enhancing polar auxin transport. *Development* **128**, 4057-4067.
Blilou, I., Xu, J., Wildwater, M., Willemsen, V., Paponov, I., Friml, J., Heidstra, R., Aida, M., Palme, K. and Scheres, B. (2005). The PIN auxin efflux facilitator network controls growth and patterning in Arabidopsis roots. *Nature* **433**, 39-44.
Casimiro, I., Marchant, A., Bhalerao, R. P., Beeckman, T., Dhooge, S., Swarup, R., Graham, N., Inzé, D., Sandberg, G., Casero, P. J. et al. (2001). Auxin transport promotes Arabidopsis lateral root initiation. *Plant Cell* **13**, 843-852.
de Reuille, P. B., Bohn-Courseau, I., Ljung, K., Morin, H., Carraro, N., Godin, C. and Traas, J. (2006). Computer simulations reveal properties of the cell-cell signaling network at the shoot apex in Arabidopsis. *Proc. Natl. Acad. Sci. USA* **103**, 1627-1632.
Dhonukshe, P., Aniento, F., Hwang, I., Robinson, D. G., Mravec, J., Stierhof, Y. D. and Friml, J. (2007). Clathrin-mediated constitutive endocytosis of PIN auxin efflux carriers in Arabidopsis. *Curr. Biol.* **17**, 520-527.
Feugier, F. G. and Iwasa, Y. (2006). How canalization can make loops: a new model of reticulated leaf vascular pattern formation. *J. Theor. Biol.* **243**, 235-244.
Feugier, F. G., Mochizuki, A. and Iwasa, Y. (2005). Self-organization of the vascular system in plant leaves: inter-dependent dynamics of auxin flux and carrier proteins. *J. Theor. Biol.* **236**, 366-375.
Friml, J. (2003). Auxin transport – shaping the plant. *Curr. Opin. Plant Biol.* **6**, 7-12.
Friml, J., Yang, X., Michniewicz, M., Weijers, D., Quint, A., Tietz, O., Benjamins, R., Ouwerkerk, P. B. F., Ljung, K., Sandberg, G. et al. (2004). A PINOID-dependent binary switch in apical-basal PIN polar targeting directs auxin efflux. *Science* **306**, 862-865.
Fujita, H. and Mochizuki, A. (2006). Pattern formation of leaf veins by the positive feedback regulation between auxin flow and auxin efflux carrier. *J. Theor. Biol.* **241**, 541-551.
Gälweiler, L., Guan, C., Müller, A., Wisman, E., Mendgen, K., Yephremov, A. and Palme, K. (1998). Regulation of polar auxin transport by AtPIN1 in Arabidopsis vascular tissue. *Science* **282**, 2226-2230.
Garnett, P., Steinacher, A., Stepney, S., Clayton, R. and Leyser, O. (2010). Computer simulation: the imaginary friend of auxin transport biology. *BioEssays* **32**, 828-835.
Geldner, N., Friml, J., Stierhof, Y. D., Jürgens, G. and Palme, K. (2001). Auxin transport inhibitors block PIN1 cycling and vesicle trafficking. *Nature* **413**, 425-428.
Grieneisen, V. A., Xu, J., Marée, A. F. M., Hogeweg, P. and Scheres, B. (2007). Auxin transport is sufficient to generate a maximum and gradient guiding root growth. *Nature* **449**, 1008-1013.
Heisler, M. G. and Jönsson, H. (2006). Modeling auxin transport and plant development. *J. Plant Growth Regul.* **25**, 302-312.
Heisler, M. G., Hamant, O., Krupinski, P., Uyttewaal, M., Ohno, C., Jönsson, H., Traas, J. and Meyerowitz, E. M. (2010). Alignment between PIN1 polarity and microtubule orientation in the shoot apical meristem reveals a tight coupling between morphogenesis and auxin transport. *PLoS Biol.* **8**, e1000516.
Jönsson, H. and Krupinski, P. (2010). Modeling plant growth and pattern formation. *Curr. Opin. Plant Biol.* **13**, 5-11.
Jönsson, H., Heisler, M. G., Shapiro, B. E., Meyerowitz, E. M. and Mjolsness, E. (2006). An auxin-driven polarized transport model for phyllotaxis. *Proc. Natl. Acad. Sci. USA* **103**, 1633-1638.
Kramer, E. M. (2008). Computer models of auxin transport: a review and commentary. *J. Exp. Bot.* **59**, 45-53.
Kramer, E. M. (2009). Auxin-regulated cell polarity: an inside job? *Trends Plant Sci.* **14**, 242-247.
Merks, R. M. H., Van de Peer, Y., Inzé, D. and Beemster, G. T. S. (2007). Canalization without flux sensors: a traveling-wave hypothesis. *Trends Plant Sci.* **12**, 384-390.
Michniewicz, M., Zago, M. K., Abas, L., Weijers, D., Schweighofer, A., Meskiene, I., Heisler, M. G., Ohno, C., Zhang, J., Huang, F. et al. (2007). Antagonistic regulation of PIN phosphorylation by PP2A and PINOID directs auxin flux. *Cell* **130**, 1044-1056.
Mitchison, G. J. (1980). A model for vein formation in higher plants. In *Proc. R. Soc. Lond. Biol. Sci.* **207**, 79-109.
Mitchison, G. J. (1981). The polar transport of auxin and vein patterns in plants. *Philos. Trans. R. Soc. B* **295**, 461-471.
Muller, A., Guan, C., Galweiler, L., Tanzler, P., Huijser, P., Marchant, A., Parry, G., Bennett, M., Wisman, E. and Palme, K. (1998). AtPIN2 defines a locus of Arabidopsis for root gravitropism control. *EMBO J.* **17**, 6903-6911.
Newell, A. C., Shipman, P. D. and Sun, Z. (2007). Phyllotaxis: cooperation and competition between mechanical and biochemical processes. *J. Theor. Biol.* **251**, 421-439.
Paciorek, T., Zazímalová, E., Ruthardt, N., Petrásek, J., Stierhof, Y. D., Kleine-Vehn, J., Morris, D. A., Emans, N., Jürgens, G., Geldner, N. et al. (2005). Auxin inhibits endocytosis and promotes its own efflux from cells. *Nature* **435**, 1251-1256.
Paponov, I. A., Teale, W. D., Trebar, M., Blilou, I. and Palme, K. (2005). The PIN auxin efflux facilitators: evolutionary and functional perspectives. *Trends Plant Sci.* **10**, 170-177.
Petrásek, J., Mravec, J., Bouchard, R., Blakeslee, J. J., Abas, M., Seifertová, D., Wisniewska, J., Tadele, Z., Kubes, M., Covanová, M. et al. (2006). PIN proteins perform a rate-limiting function in cellular auxin efflux. *Science* **312**, 914-918.
Reinhardt, D., Mandel, T. and Kuhlemeier, C. (2000). Auxin regulates the initiation and radial position of plant lateral organs. *Plant Cell* **12**, 507-518.
Reinhardt, D., Pesce, E. R., Stieger, P., Mandel, T., Baltensperger, K., Bennett, M., Traas, J., Friml, J. and Kuhlemeier, C. (2003). Regulation of phyllotaxis by polar auxin transport. *Nature* **426**, 255-260.
Robert, S., Kleine-Vehn, J., Barbez, E., Sauer, M., Paciorek, T., Baster, P., Vanneste, S., Zhang, J., Simon, S., Čovanová, M. et al. (2010). ABP1 mediates auxin inhibition of clathrin-dependent endocytosis in Arabidopsis. *Cell* **143**, 111-121.
Rolland-Lagan, A. G. and Prusinkiewicz, P. (2005). Reviewing models of auxin canalization in the context of leaf vein pattern formation in Arabidopsis. *Plant J.* **44**, 854-865.
Sabatini, S., Beis, D., Wolkenfelt, H., Murfett, J., Guilfoyle, T., Malamy, J., Benfey, P., Leyser, O., Bechtold, N., Weisbeek, P. et al. (1999). An auxin-dependent distal organizer of pattern and polarity in the Arabidopsis root. *Cell* **99**, 463-472.

Sachs, T. (1969). Polarity and the induction of organized vascular tissues. *Ann. Bot. (Lond.)* **33**, 263-275.
Sahlin, P., Söderberg, B. and Jönsson, H. (2009). Regulated transport as a mechanism for pattern generation: capabilities for phyllotaxis and beyond. *J. Theor. Biol.* **258**, 60-70.
Scarpella, E., Marcos, D., Friml, J. and Berleth, T. (2006). Control of leaf vascular patterning by polar auxin transport. *Genes Dev.* **20**, 1015-1027.
Smith, R. S., Guyomarc'h, S., Mandel, T., Reinhardt, D., Kuhlemeier, C. and Prusinkiewicz, P. (2006). A plausible model of phyllotaxis. *Proc. Natl. Acad. Sci. USA* **103**, 1301-1306.
Stoma, S., Lucas, M., Chopard, J., Schaedel, M., Traas, J. and Godin, C. (2008). Flux-based transport enhancement as a plausible unifying mechanism for auxin transport in meristem development. *PLoS Comput. Biol.* **4**, e1000207.
Swarup, R., Marchant, A. and Bennett, M. J. (2000). Auxin transport: providing a sense of direction during plant development. *Biochem. Soc. Trans.* **28**, 481-485.
Vieten, A., Vanneste, S., Wisniewska, J., Benkova, E., Benjamins, R., Beeckman, T., Luschnig, C. and Friml, J. (2005). Functional redundancy of PIN proteins is accompanied by auxin-dependent cross-regulation of PIN expression. *Development* **132**, 4521-4536.
Wabnik, K., Kleine-Vehn, J., Balla, J., Sauer, M., Naramoto, S., Reinöhl, V., Merks, R. M., Govaerts, W. and Friml, J. (2010). Emergence of tissue polarization from synergy of intracellular and extracellular auxin signaling. *Mol. Syst. Biol.* **6**, 447.
Wabnik, K., Govaerts, W., Friml, J. and Kleine-Vehn, J. (2011). Feedback models for polarized auxin transport: an emerging trend. *Mol. Biosyst.* **7**, 2352-2359.
Wisniewska, J., Xu, J., Seifertová, D., Brewer, P. B., Ruzicka, K., Blilou, I., Rouguié, D., Benková, E., Scheres, B. and Friml, J. (2006). Polar PIN localization directs auxin flow in plants. *Science* **312**, 883.

Supplementary material: Self-organising proporties of polar auxin transport

Klaartje van Berkel[1,2], Rob J. de Boer[2], Ben Scheres[1], Kirsten ten Tusscher[2]

[1]Molecular Genetics Group, Department of Biology, Utrecht University, Padualaan 8, 3584 CH Utrecht, The Netherlands

[2]Theoretical Biology Group, Department of Biology, Utrecht University, Padualaan 8, 3584 CH Utrecht, The Netherlands

S.1 Phase plane analysis

To study the dynamic behaviour of the simplified models we use the so-called method of phase plane analysis (figure S.1, table S.1) . This method can be applied if the model consists of two variables (P and A at membrane segment level) or when the model has been further simplified to two variables (P_0 and P_1 at single cell level, when auxin dynamics are assumed to be in quasi steady state). The major idea behind the method of phase plane analysis is to depict the dynamics of the two model variables in a 2-dimensional plane (the phase plane).

Consider a general model with two variables x and y, whose dynamics are typically dependent on each other (e.g. P and A or P_0 and P_1). For this model system we can draw a phase plane with x on the horizontal and y on the vertical axis. Each point in this phase plane represents a potential state of the model system, its coordinates representing the values of x and y in this state. In this phase plane we can depict the dynamics of the variables at each point, using horizontal arrows to depict increases ($\rightarrow$) and decreases ($\leftarrow$) in x and vertical arrows to depict increases ($\uparrow$) and decreases ($\downarrow$) in y. Together these arrows constitute a vector field (note that we can determine the dynamics of x and y in a point simply from the values of $\frac{dx}{dt}$ and $\frac{dy}{dt}$ in that point).

A phase plane contains two (sets of) equilibrium lines, also named isoclines, for which one of the variables does not change in time. These lines are obtained by setting the equation $\frac{dx}{dt}$ or $\frac{dy}{dt}$, respectively, equal to 0. The vector field for each variable switches sign when crossing the respective equilibrium line. Change of this variable is either positive (growth) below or to the left of the equilibrium line and negative (decrease) above or to the right, or *vice versa*. When these equilibrium lines intersect, both variables are in steady state and an equilibrium occurs. Equilibria can be stable (figure S.1**A**) or unstable (figure S.1**B**). When a system that is in a stable equilibrium is perturbed, it will move back to this equilibrium. When the equilibrium is unstable, a perturbation will cause the system to move away from it. Stability of equilibria can often be determined directly by looking at the vector field: if all arrows point towards the equilibrium it is stable, if one or more arrows point away from the equilibrium it is unstable.

A crucial point in our analysis is the distinction between systems with one and systems with multiple stable states. In systems with a single stable equilibrium the system's state will in the long run converge to that equilibrium. In contrast, in bistable system where two stable equilibria are separated by an unstable equilibrium the initial conditions of the system determine to which of the two stable equilibria the system converges (figure S.1**C**).

S.1.1 Difference between single equilibrium and bistable system

Figure S.2 illustrates the differences in behaviour at the single cell level between a system with one stable equilibrium and a bistable system. In the absence of transient perturbations or an external gradient (fig S.2**A** and **D**), the system can be in a symmetric equilibrium in which $P_0 = P_1$. When transiently perturbed from this symmetric

Table S.1: Summary of terms

term	meaning
system	one or more coupled variables for which a differential equation describes the change over time
phase plane (2D)	all possible combinations of x and y values i.e. all possible states of the system
vector field	representation of direction of change for each variable at each position in the phase plane
equilibrium line, isocline	x and y values for which one of the variables does not change
equilibrium	point in which two equilibrium lines intersect and both variables do not change
stable equilibrium, attractor	equilibrium to which a system converges
unstable equilibrium	equilibrium from which a system diverges when perturbed
bistability	situation in which a system has two stable equilibria, separated by an unstable one; or more generally a situation in which a system has an unstable equilibrium separating two distinct long term attractors of the system
PAT model interpretation	
bistability (membrane segment)	a membrane segment either has high or low concentration of PIN proteins
polarity (cell)	a single cell contains at least one membrane segment with high PIN concentration and at least one with low PIN concentration
gradient-driven pattern formation (tissue)	cells within the tissue are not polar, constant sources and sinks keep patterns intact
self-organisation (tissue)	externally applied biases like sources and sinks are not required to maintain a pattern
polarity-driven self-organisation (tissue)	self-organisation results from the ability of single cells to polarise

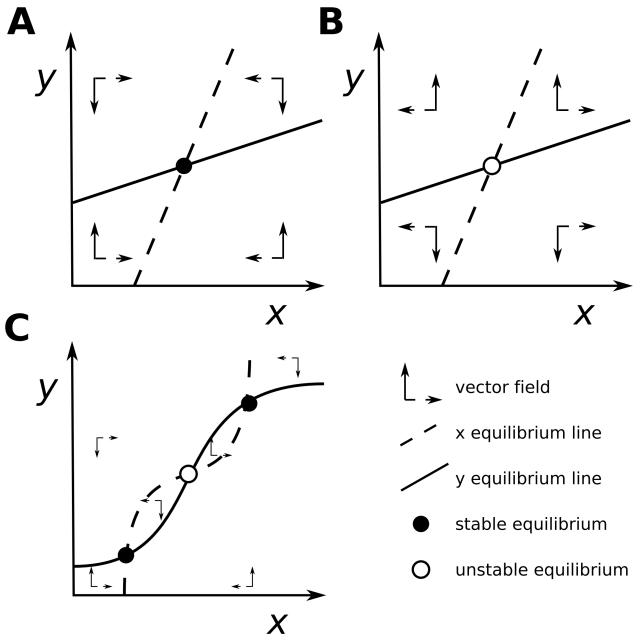

Figure S.1: Examples of phase planes of x and y. Two arbitrary straight equilibrium lines intersect once, providing one equilibrium (**A** and **B**). Depending on the equations (not shown) the vector field can point toward (**A**) or away (**B**) from the equilibrium, i.e. the equilibrium is either stable or unstable. **C**: example of a bistable system. The two equilibrium lines intersect three times. The vector field shows that the outer two equilibria are stable whereas the middle one is unstable.

equilibrium by increasing P_0 (red dots in fig S.2**B** and **E**), the single equilibrium system will eventually return to its symmetrical equilibrium (fig S.2**B**) whereas the bistable system will leave its unstable symmetrical equilibrium and converge to the stable polar equilibrium in which P_0 is high and P_1 is low (fig **S.2E**). Figure **C** shows in red how the phase plane of the single equilibrium model changes when the cell lies in an external auxin gradient. Due to the gradient the membranes of the cells now experience different auxin concentrations, causing P_0 and P_1 to become different from each other such that the single stable equilibrium is no longer symmetrical ($P_0 > P_1$, or *vice versa* in case of the opposite gradient). Figure F shows in red how the phase plane changes for the bistable model when the cell lies in an auxin gradient. We see that the region of the phase plane for which the system will converge to the $P_0 \gg P_1$ polar state (boundary of which is given by the dotted line) becomes larger and now includes the symmetrical initial conditions. Now, even when the cell is initiated in a uniform, symmetrical, state, it will polarise. Note that the polar stable equilibria in fig S.2**D-F** are fundamentally different from the somewhat polarised state in **C**. In the former case, the system is strictly polar, whereas the different concentrations of P_0 and P_1 obtained in the latter are a direct result of the external auxin gradient.

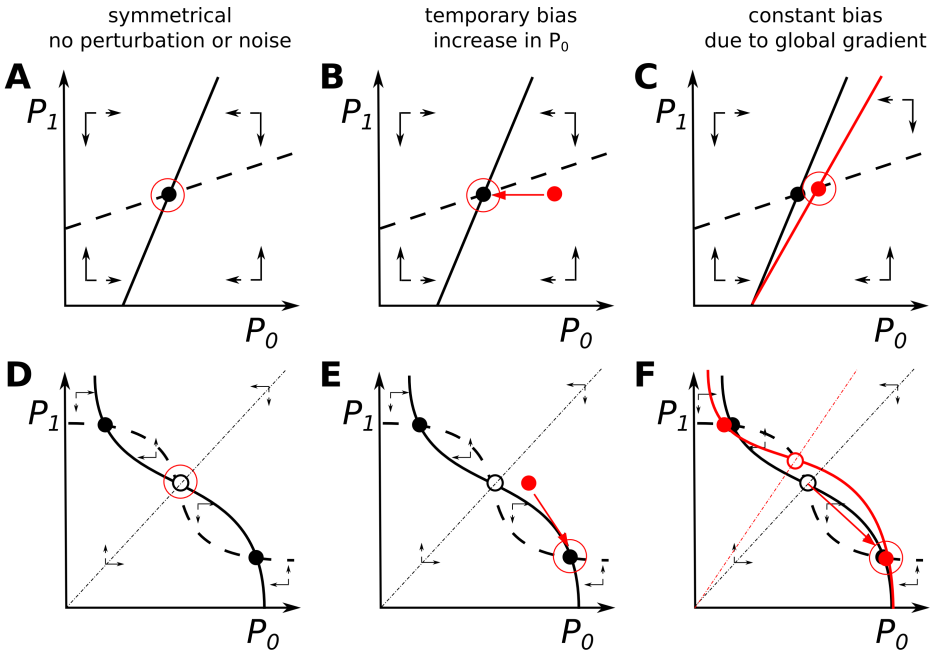

Figure S.2: Phase planes of single equilibrium (**A**-**C**) and bistable (**D**-**F**) single cell models and reactions to temporal perturbations or a global gradient. **A** and **D**: no perturbations or gradient present. **B** and **E**: phase plane after perturbation by increasing the level of P_0. **C** and **F**: change of phase plane when a constant global gradient is present. Solid equilibrium lines are for P_0, dotted equilibrium lines are for P_1. The equilibrium to which a system converges is markes with a large red circle. Red dots in **B** and **E** are initial conditions in which P_0 is slightly increased. In **C** and **F**, altered equilibrium lines and equilibria are marked in red.

S.2 Mathematical framework to study PAT models

S.2.1 Membrane segment model analysis

The caricature membrane segment model consists of an equation for the PIN level at the membrane segment (P) and and equation for auxin in the adjoining neighbouring cell (A). All other PIN and auxin concentrations are assumed to be constant. We use these two variables for all discussed models, but take into account the specific mathematical details of individual models. All phase planes are drawn with P on the y- and A on the x-axis. However, in some cases it is much easier to write A as a function of P.

The default auxin equation is given by:

$$\frac{dA}{dt} = p + i_{pas} + i_{pin}P - eA - dA \tag{S.1}$$

p and d are the production and decay rates respectively. i_{pas} is the passive and $i_{pin}P$ the active rate of influx over the membrane of interest and into the neighbouring cell. Efflux occurs at rate e. A number of models takes into account saturation of auxin transport through the PIN proteins. In our caricature membrane segment model, this translates into:

$$\frac{dA}{dt} = p + i_{pas} + i_{pin}P - (e_{pas} + \frac{e_{pin}}{h_{pin} + A})A - dA \tag{S.2}$$

Note that the $i_{pin}P$ term is not affected, since auxin concentration in the cell to which the membrane segment belongs is assumed to be constant. Instead, we split up the efflux from the neighbouring cell of interest into

a passive (e_{pas}) and active efflux (e_{pin}), the latter of which saturates with the auxin concentration and is half maximum when $A = h$.

The auxin equilibrium line is obtained by setting $\frac{dA}{dt} = 0$. The default auxin equilibrium line is given by (eq 1 in box 1 in the main text):

$$P = \frac{(e+d)A - p - i_{pas}}{i_{pin}} \tag{S.3}$$

If PIN-mediated efflux is saturated, the auxin equilibrium line is given by:

$$P = \frac{(e_{pas} + \frac{e_{pin}}{h_{pin}+A} + d)A - p - i_{pas}}{i_{pin}} \tag{S.4}$$

Ignoring auxin feedback on PIN dynamics for a moment, the equation for PIN dynamics can be written as (eq 3 in box 1 in the main text):

$$\frac{dP}{dt} = k_{on} - k_{off}P \tag{S.5}$$

Depending on the type of feedback of auxin on PIN dynamics, either exocytosis rate k_{on} or endocytosis rate k_{off} depend on auxin flux or concentration.

The assumption of a limiting PIN pool affects PIN dynamics as the membrane segment of interest depletes the pool and thus inhibits its own availability of PINs. This alters the PIN equation to:

$$\frac{dP}{dt} = k_{on}(P_{tot} - P) - k_{off}P \tag{S.6}$$

In which P_{tot} is the total amount of PINs the cell contains. In some models the cytosolic PIN pool is modeled dynamically.

S.2.2 Single cell model analysis

Our single cell model consists of one cell containing PIN levels on two membrane segments (P_0 and P_1) and auxin levels in the two corresponding neighbouring cells (A_0 and A_1). As for the membrane segment model, all other PIN and auxin concentrations are assumed to be constant. Equations for auxin are the same as for the membrane segment model (eq S.1 or S.2) and the same is true for the PIN equation if there is no limiting PIN pool (equation S.5). If there is a PIN pool, it is now depleted by both membrane segments:

$$\frac{dP_i}{dt} = k_{on}(P_{tot} - \sum_n P_i) - k_{off}P_i \quad \text{with } i = 0, 1 \tag{S.7}$$

with n being the total number of membrane segments belonging to one cell. In order to simplify this 4 variable model into a 2 variable model that we can analyse using the phase plane method, we assume that auxin dynamics are fast and hence are in steady state. This allows us to use a so-called quasi steady state (QSS) assumption for auxin dynamics, setting the auxin differential equations to 0. For the simplest auxin equation (eq S.1) we then find:

$$A_i = \frac{p + i_{pas} + i_{pin}P_i}{e+d} \tag{S.8}$$

Substituting equation S.8 in the PIN equations now leaves us with a 2-variable system that we can study with phase plane analysis. Hence, most single cell phase planes will have P_1 on the y- and P_0 on the x-axis. In some cases, however, the authors have already implemented a QSS for the PIN equations and we draw a phase plane for A_1 and A_0 instead.

S.2.3 Concentration, flux and the shape of the PIN equilibrium line

To determine the precise shape of the PIN equilibrium lines in both the membrane segment and single cell models we need to fill in the feedback of auxin on PIN cycling dynamics. Feedback of auxin on membrane PIN levels occurs in most models through either auxin concentrations in neighbouring cells or through auxin fluxes across the membrane.

S.2.3.1 Concentration-based feedback

First let us consider a few elementary shapes for the function describing feedback of auxin concentration on PIN cycling. We use the example of feedback through k_{on}. Feedback on k_{off} will give similar results. A number of ways in which k_{on} might depend on auxin concentration in the neighbouring cell are: linear ($k_{on} = k_{on_b} + k_{on_f} A$), superlinear (e,g, quadratic, $k_{on} = k_{on_b} + k_{on_f} A^2$) or saturating with A ($k_{on} = k_{on_b} + \frac{k_{on_b} A^n}{h_A^n + A^n}$). In all cases, k_{on_b} is the basal exocytosis rate, k_{on_f} is the extra exocytosis rate that depends on auxin. In case of the saturating feedback h_A is the auxin concentration for which k_{on} is half maximum. If $n > 1$, the saturation is sigmoid.

Substituting these into the PIN equation without a limiting PIN pool (eq S.5) and putting it to zero would produce the following PIN equilibrium lines (all phase planes are shown in fig S.3 with a reference to the equation that produces the PIN equilibrium line):

1: linear feedback and unlimiting PIN pool:

$$P = \frac{k_{on_b} + k_{on_f} A}{k_{off}} \tag{Conc.1.a}$$

2: quadratic feedback and unlimiting PIN pool:

$$P = \frac{k_{on_b} + k_{on_f} A^2}{k_{off}} \tag{Conc.2.a}$$

3: saturating feedback and unlimiting PIN pool:

$$P = \frac{k_{on_b}}{k_{off}} + \frac{k_{on_f} A^n}{k_{off}(h_A^n + A^n)} \tag{Conc.3.a}$$

If instead the PIN pool is limiting (eq S.6), the PIN equilibrium lines become:

4: linear feedback and limiting PIN pool:

$$P = \frac{P_{tot}(k_{on_b} + k_{on_f} A)}{k_{off} + k_{on_b} + k_{on_f} A} \tag{Conc.1.b}$$

5: quadratic feedback and limiting PIN pool:

$$P = \frac{P_{tot}(k_{on_b} + k_{on_f} A^2)}{k_{off} + k_{on_b} + k_{on_f} A^2} \tag{Conc.2.b}$$

6: saturating feedback and limiting PIN pool:

$$P = \frac{P_{tot}(k_{on_b} h_A^n + (k_{on_b} + k_{on_f}) A^n)}{((k_{on_b} + k_{off}) h_A^n + (k_{on_b} + k_{on_f} + k_{off}) A^n)} \tag{Conc.3.b}$$

Hence, the addition of a limiting PIN pool effectively alters the linear PIN equilibrium (eq Conc.1.a) line into a line that saturates with auxin (eq Conc.1.b) and the quadratic PIN equilibrium (eq Conc.2.a) line into a sigmoid one (eq Conc.2.b). If the feedback was already saturating, the limiting PIN pool changes the exact position, but not the shape of the PIN equilibrium line (compare eq Conc.3.a and eq Conc.3.b).

S.2.3.2 Flux-based feedback

In order to fill in the feedback of auxin flux on PIN cycling we first need to formulate an expression for across membrane auxin flux, which we will derive here. Both at the membrane segment and single cell level we study PIN concentrations at a membrane segment and the auxin concentration in the corresponding neighbouring cell. Flux is regarded with respect to the membrane segment(s) of interest and is positive in case of net efflux and negative in case of net influx. Hence the equation for (non-saturating) flux (F) is:

$$F = i_{pas} + i_{pin}P - eA \tag{S.9}$$

Note that we use the same nomenclature as for the auxin in the neighbouring cell (i_{pas} and i_{PIN} are influxes into the neighbouring cell and effluxes over the membrane segment of interest, e is efflux from the neighbouring cell and influx over the membrane segment of interest). Similarly, since the focus is on the membrane segment (with PIN level P) and its neighbouring cell (with auxin level A), the auxin in the cell to which the membrane segment belongs is assumed to be constant, and is incorporated in i_{pas} and i_{pin}. Most flux-based models assume that only net efflux feeds back on PIN localisation, using a Heaviside function $\theta(F)$ to switch feedback on if flux is positive and off if flux is negative.

Now let us consider the same elementary shapes for flux feedback functions and the PIN equilibrium lines they produce. It is important to notice that when calculating the flux, both P and A are taken into account. Hence, if flux feeds back on PIN cycling, the PIN concentration feeds back on itself.

1: linear feedback ($k_{on} = k_{on_b} + k_{on_f}\theta(F)F$) and unlimiting PIN pool:

$$P = \begin{cases} \frac{k_{on_b}}{k_{off}} & \text{if } F \leq 0 \\ \frac{k_{on_f}(eA - i_{pas}) - k_{on_b}}{k_{on_f} i_{pin} - k_{off}} & \text{if } F > 0 \end{cases} \tag{Flux.1.a}$$

2: quadratic feedback ($k_{on} = k_{on_b} + k_{on_f}\theta(F)F^2$) and unlimiting PIN pool:

$$P = \begin{cases} \frac{k_{on_b}}{k_{off}} & \text{if } F \leq 0 \\ \frac{2k_{on_f} i_{pin}(eA - i_{pas}) + k_{off} + \sqrt{4k_{on_f} k_{off} i_{pin}(eA - i_{pas}) + k_{off}^2 - 4k_{on_f} i_{pin}^2 k_{on_b}}}{2k_{on_f} i_{pin}^2} & \text{if } F > 0 \end{cases} \tag{Flux.2.a}$$

3: saturating feedback ($k_{on} = k_{on_b} + k_{on_f}\theta(F)\frac{F^n}{h_F^n + F^n}$) and unlimiting PIN pool:

$$\begin{cases} P = \frac{k_{on_b}}{k_{off}} & \text{if } F \leq 0 \\ A = \frac{1}{e}\left(i_{pas} + i_{pin}P + \sqrt[n]{\frac{h_F^n (k_{off}P - k_{on_b})}{k_{off}P - k_{on_b} - k_{on_f}}} \right) & \text{if } F > 0 \end{cases} \tag{Flux.3.a}$$

And, as well, with limiting PIN pool:

4: linear feedback and limiting PIN pool:

$$\begin{cases} P = \frac{k_{on_b} P_{tot}}{k_{off} + k_{on_b}} & \text{if } F \leq 0 \\ A = \frac{k_{on_f}(i_{pas}P + i_{pin}P^2 - i_{pin}P_{tot}P - i_{pas}P_{tot}) - k_{on_b}(P_{tot} - P) + k_{off}P}{k_{on_f} e (P - P_{tot})} & \text{if } F > 0 \end{cases} \tag{Flux.1.b}$$

5: quadratic feedback and limiting PIN pool:

$$\begin{cases} P = \frac{k_{on_b} P_{tot}}{k_{off} + k_{on_b}} & \text{if } F \leq 0 \\ A = \frac{k_{on_f}((i_{pas} + i_{pin}P)(P - P_{tot}) + \sqrt{-k_{on_f}((P - P_{tot})(k_{on_b}P + k_{off}P - k_{on_b}P_{tot}))}}{k_{on_f}(P - P_{tot})e} & \text{if } F > 0 \end{cases} \tag{Flux.2.b}$$

6: saturating feedback and limiting PIN pool:

$$\begin{cases} P = \frac{k_{on_b} P_{tot}}{k_{off} + k_{on_b}} & \text{if } F \leq 0 \\ A = \frac{1}{e}\left(i_{pas} + i_{pin}P - \sqrt[n]{\frac{h_F^n (k_{on_b}P + k_{off}P - k_{on_b}P_{tot})}{k_{on_b}(P_{tot} - P) + k_{on_f}(P_{tot} - P) - k_{off}P}} \right) & \text{if } F > 0 \end{cases} \tag{Flux.3.b}$$

In all cases, the Heaviside function $\theta(F)$ causes a sharp switch in the PIN equilibrium line, which makes it inherently non-linear. The limiting PIN pool causes the PIN equilibrium line to curve back, such that it becomes a sigmoid-like line.

S.3 Membrane segment variants

Here we present an overview of distinct model behaviours at the membrane segment level for all possible combinations of auxin and PIN dynamics. At the membrane segment we can distinguish between systems with one, two (semi-bistable) or three (bistable) equilibria. Different combinations of auxin and PIN equilibrium lines can lead to one of these cases:

MS.I: straight A equilibrium line and (sub)linear P equilibrium line: one equilibrium If the straight A equilibrium line that results from our default auxin equation S.1 is combined with a PIN equilibrium line that is linear or saturates with $n = 1$ (eq Conc.1.a, Conc.1.b, Conc.3.a and Conc.3.b), there can be only one stable equilibrium, and thus no bistability (fig S.3**A**) independent of whether or not a limiting PIN pool is assumed.

MS.II: straight A equilibrium line and superlinear P equilibrium line: two equilibria When the auxin equilibrium line is a straight line (eq S.3 as follows from the auxin eq S.1), bistability can occur when the PIN equilibrium line is superlinear and non-saturating (eq Conc.2.a, Flux.1.a and Flux.2.a). There are two equilibria. The lower equilibrium is stable and the upper unstable. Above the upper equilibrium there is a region of unlimited increase of PIN levels. This situation results in a bistable system, since it has two regions of distinctly different behaviour, even though there is only one stable equilibrium (fig S.3**B**) and an unlimiting PIN pool is assumed.

MS.III: straight A equilibrium line and sigmoid P equilibrium line: three equilibria A straight auxin equilibrium line can intersect thrice with a sigmoid PIN equilibrium line (eq Conc.3.a with $n = 2$, **Conc.2.b**, **Conc.3.b** with $n = 2$, **Flux.1.b**, **Flux.2.b**, **Flux.3.a** and **Flux.3.b**) (fig S.3**C**). The outer two equilibria are stable and the middle one is unstable. Hence, bistability arises from a sigmoid saturating feedback or a non-linear feedback combined with a limiting PIN pool.

MS.IV: both A and P equilibrium lines are non-linear: two or three equilibria Non-linearity in the auxin equilibrium line (eq S.4) can introduce bistability when combined with a PIN equilibrium line that previously would not give bistability (eq **Conc.3.a** with $n = 1$, **Conc.1.b**, **Conc.3.b** with $n = 1$) (fig S.3**D**).

S.4 Single cell variants

At the cell level we are interested in whether the system can display polar behaviour. For this the model needs to have two stable polar equilibria, one with high PIN levels on one membrane segment and low PIN levels on the other and one *vice versa*. The different possible combinations of model assumptions produce a total of three different scenarios, for two of which cell polarity can occur.

SC.I: non-bistable membrane segments combined with a limiting PIN pool: no polarity As an example of this scenario, consider the concentration-based, linear, feedback that is not able to give membrane bistability. Combining this feedback with a limiting PIN pool gives the following PIN equations for P_0 and P_1:

$$\frac{dP_i}{dt} = (k_{on_b} + k_{on_f} A_i)(P_{tot} - P_i - P_j) - k_{off} P_i \quad \text{with } i = 0, 1 \text{ and } j = 1, 0 \tag{S.10}$$

Substituting the auxin QSS, to reduce the system to two variables gives us the full PIN equation:

$$\frac{dP_i}{dt} = \left(k_{on_b} + k_{on_f} \left(\frac{p + i_{pas} + i_{pin} P_i}{e + d}\right)\right)(P_{tot} - P_i - P_j) - k_{off} P_i \quad \text{with } i = 0, 1 \text{ and } j = 1, 0 \tag{S.11}$$

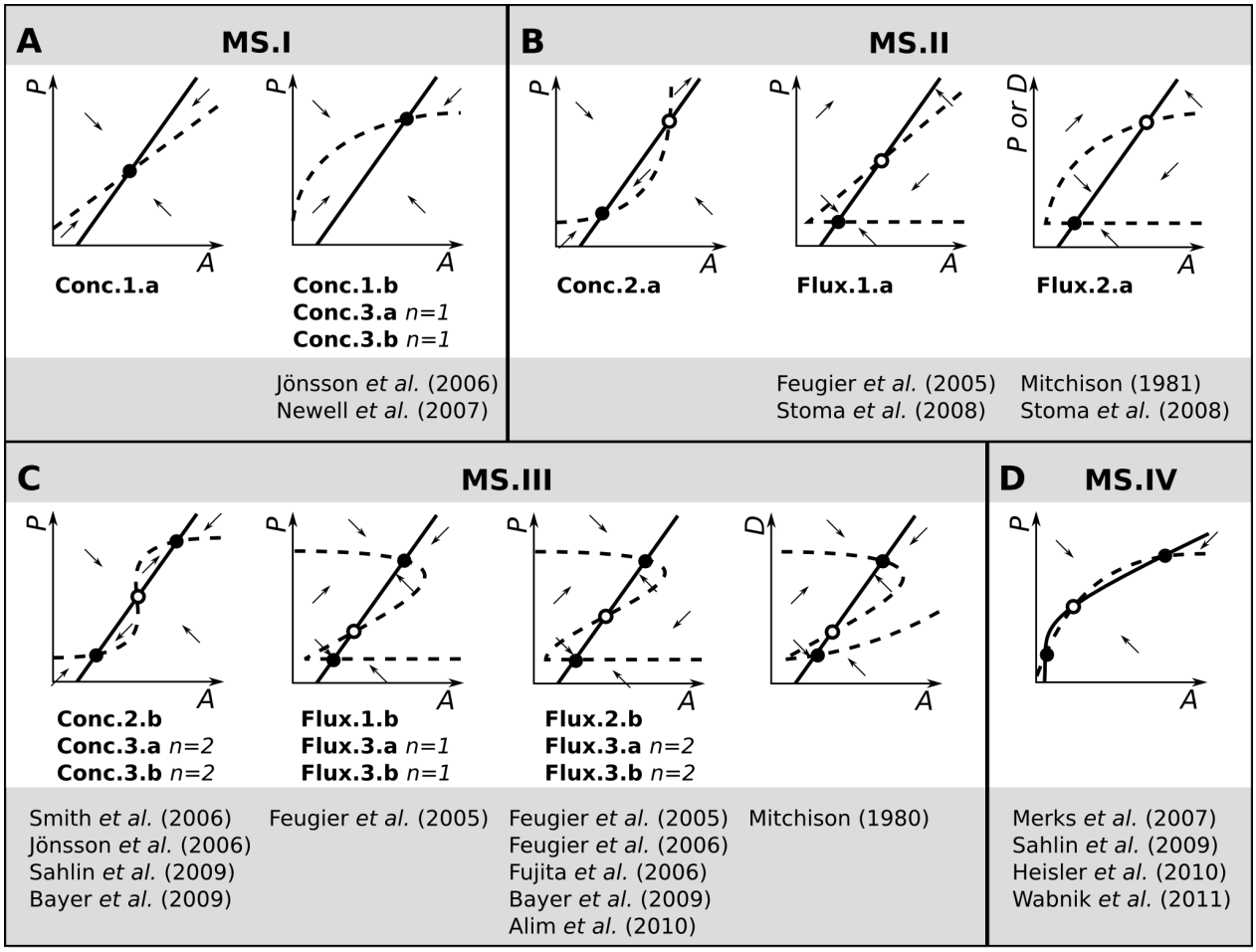

Figure S.3: Overview of the different membrane segment variants with corresponding PIN equilibrium lines and references to PAT models with (similar) auxin and PIN dynamics. Dashed lines: P equilibrium lines. Solid lines: A equilibrium lines. Closed circles: unstable equilibria. Open circles: stable equilibria. Arrows represent the direction of dynamics.

The resulting equilibrium lines are shown in fig S.4**A** Although P_0 and P_1 are interdependent, their equilibrium lines are only able to intersect once in a stable equilibrium in which (given no external bias) $P_0 = P_1$. Hence, no cell polarity occurs.

SC.II: bistability at the membrane segment level combined with a limiting PIN pool: polarity (+ rest state) As an example of this scenario, consider the concentration-based, quadratic, feedback as in equation Conc.2.b. Implementing this feedback at the single cell level gives us the following PIN equations for P_0 and P_1:

$$\frac{dP_i}{dt} = (k_{on_b} + k_{on_f} A_i^2)(P_{tot} - P_i - P_j) - k_{off} P_i \quad \text{with } i = 0,1 \text{ and } j = 1,0 \tag{S.12}$$

Substituting the auxin QSS gives us the full PIN equation:

$$\frac{dP_i}{dt} = \left(k_{on_b} + k_{on_f} \left(\frac{p + i_{pas} + i_{pin} P_i}{e + d}\right)^2\right)(P_{tot} - P_i - P_j) - k_{off} P_i \quad \text{with } i = 0,1 \text{ and } j = 1,0 \tag{S.13}$$

The resulting equilibrium lines can intersect three times (fig S.4**B**). Two of these equilibria are stable and asymmetrical ($P_0 > P_1$ and $P_0 < P_1$), one is unstable and symmetrical ($P_0 \sim P_1$). If a model contains only these three equilibria it polarises automatically due to noise.

Additionally, a third stable equilibrium, and corresponding unstable equilibria, might occur. This happens in case feedback is concentration-based and sigmoid (eq **Conc.3.b** with $n = 2$) and in case of flux-based feedback (due to the Heaviside function). This third equilibrium occurs for $P_0 = P_1$ and represents an apolar rest state. The system has to be sufficiently perturbed from this state in order to become polar.

SC.III: non-bistable membrane segments combined with an unlimiting PIN pool: no polarity As an example, if the linear concentration-based feedback (eq **Conc.1.a**) is combined with an unlimiting PIN pool, the PIN equations become:

$$\frac{dP_i}{dt} = k_{on_b} + k_{on_f} A_i - k_{off} P_i \quad \text{with } i = 0,1 \tag{S.14}$$

Implementing the QSS for A_i gives us the full PIN equations:

$$\frac{dP_i}{dt} = k_{on_b} + k_{on_f} \left(\frac{p + i_{pas} + i_{pin} P_i}{e + d}\right) - k_{off} P_i \quad \text{with } i = 0,1 \tag{S.15}$$

And the resulting PIN equilibrium line:

$$P_i = \frac{k_{on_b}(e + d) + k_{on_f}(p + i_{pas})}{k_{off}(e + d) - k_{on_f} i_{pin}} \quad \text{with } i = 0,1 \tag{S.16}$$

Since this equilibrium line is a mere combination of parameters, it is an exactly horizontal or vertical line in the phase plane. The two equilibrium lines can, thus, only intersect once (fig S.4**C**). The intersection point is a stable equilibrium in which (given no external bias) $P_0 = P_1$. Hence, no cell polarity occurs.

SC.IV: bistability at the membrane segment level combined with an unlimiting PIN pool: polarity (+ rest state + bipolar state) As an example of this scenario, consider the sigmoid concentration-based feedback (**Conc.III.a** with $n = 2$) with an unlimiting PIN pool. The resulting single cell level PIN equation is:

$$\frac{dP_i}{dt} = k_{on_b} + \frac{k_{on_f} A_i^2}{h_A^2 + A_i^2} - k_{off} P_i \quad \text{with } i = 0,1 \tag{S.17}$$

Implementing the QSS for A_i and setting $\frac{dP_i}{dt}$ to 0 gives us three solutions for P_i, i.e. the PIN equilibrium lines are either three horizontal or three vertical lines. These lines intersect a total of nine times, giving rise to five unstable and four stable equilibria (fig S.4**D**). Two of the stable equilibria are polar, one represents the apolar rest state in which $P_0 = P_1$ and both are low, and the last represents a bipolar state in which $P_0 = P_1$ and both are high.

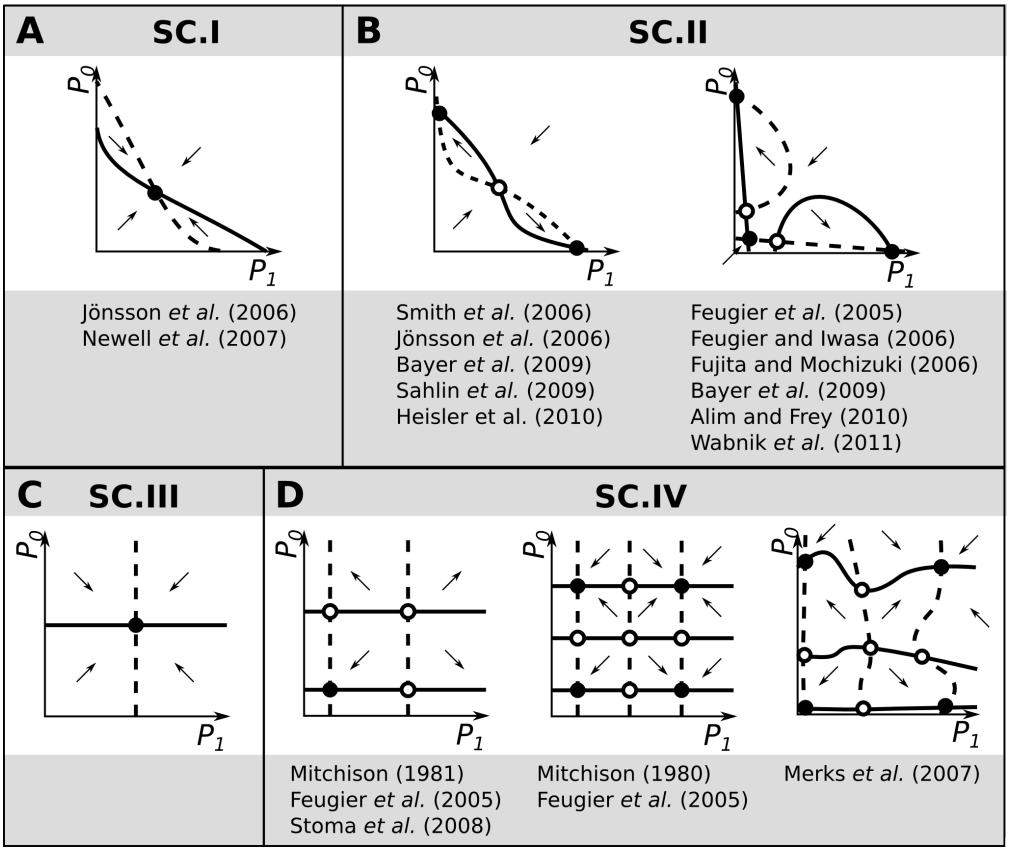

Figure S.4: Overview of the different single cell variants with references to PAT models with (similar) single cell dynamics. Solid lines: P_0 equilibrium lines. Dashed lines: P_1 equilibrium lines. Closed circles: unstable equilibria. Open circles: stable equilibria. Arrows represent the direction of dynamics.

S.5 Analysis of discussed PAT models

Here we describe how we formulated equations for PIN and auxin dynamics at the membrane segment and single cell behaviour and thus analysed model behaviour for the models discussed less extensively in the main text.

S.5.1 Flux based models

S.5.1.1 Mitchison (1980)

Mitchison [1980] developed a model in which membrane segment permeability depends on flux over that membrane. Since his model does not contain PINs, we cannot use our default auxin equation. Translating his model to our membrane segment model gives the following equation for auxin in the neighbouring cell (named "signal" in the original paper):

$$\frac{dA}{dt} = p - dA + F \tag{S.18}$$

in which p is production of the signal. In the original model, signal decay only takes place in a certain area of the tissue. In order to analyse behaviour at the membrane segment and cellular level we replace this with a decay taking place in each cell. Flux depends on the permeability of the membrane segment (D) and consists of the influx over the membrane segment of interest and efflux out of the neighbouring cell

$$F = D - eA \tag{S.19}$$

Together equation S.18 and S.19 give the auxin equilibrium line:

$$A = \frac{p + D}{e + d} \tag{S.20}$$

In turn, membrane permeability, depends on flux in a superlinear, saturating manner (membrane segment variant 1a):

$$D = \alpha \frac{F^2}{\gamma + F^2} + \beta \tag{S.21}$$

Substituting equation S.19 for F and rewriting such that A becomes a function of D gives a quadratic function. Hence, the permeability equilibrium line has two solutions:

$$A = \begin{cases} \frac{\alpha D + \beta D - D^2 + \sqrt{\alpha\gamma D - \alpha\beta\gamma - \gamma D^2 + 2\beta\gamma D - \gamma\beta^2}}{(\alpha - D + \beta)e} & \text{if } F > 0 \\ -\frac{-\alpha D - \beta D + D^2 + \sqrt{\alpha\gamma D - \alpha\beta\gamma - \gamma D^2 + 2\beta\gamma D - \gamma\beta^2}}{(\alpha - D + \beta)e} & \text{if } F \leq 0 \end{cases} \tag{S.22}$$

These two equilibrium lines (equation S.20 and S.22) can intersect in three equilibria, two of which are stable (fig S.3**C**). Hence, bistability can occur at the membrane segment level (**MS.III**).

Each membrane segment in the model determines its permeability without taking into account the other membrane segments of this cell, i.e. there is no competition for a "permeability factor" (**SC.IV**). As a result, there are 9 possible equilibria, 4 of which are stable (fig S.4**D**). Two stable equilibria are symmetrical, they represent apolar cells in which both membrane segments have a low or a high permeability. The two asymmetrical equilibria represent polar cells with a low permeability of one membrane segment and a high permeability of the other.

S.5.1.2 Mitchison (1981)

In his second model [Mitchison, 1981], Mitchison did not take into account production of auxin in individual cells, but instead allowed it to come in from a local source and redistribute along a tissue. On a similar note as above, we replaced this localised production and decay by production and decay processes taking place in each cell. The

auxin equation and auxin equilibrium line therefore remains the same with respect to the previous model (equation S.18 and S.20 respectively).

In this second model, two aspects have changed with respect to the previous model. First, direction of flux is now important. Instead of absolute flux, net efflux feeds back on D. Second, the feedback no longer saturates, but is a quadratic function. In addition, D is now a dynamic variable:

$$\frac{dD}{dt} = \alpha\theta(F)F^2 + \beta - D \tag{S.23}$$

which is equivalent to eq Flux.2.a.β is the basal flux rate over the membrane segment of interest when $F < 0$. By taking into account "degradation" of the permeability ($-D$), Mitchison already hints toward the existence of a physical pump that is subject to turnover.

D now depends as follows on flux:

$$D = \alpha\theta(F)F^2 + \beta \tag{S.24}$$

Substituting the flux and rewriting A as a function of D gives the full D equilibrium line (similar to eq Flux.2.a):

$$\begin{cases} A = \frac{\alpha D + \sqrt{-\alpha\beta + \alpha D}}{\alpha e} & \text{if } F > 0 \\ D = \beta & \text{if } F \leq 0 \end{cases} \tag{S.25}$$

which can intersect twice with the auxin equilibrium line (fig S.3**B**). The bottom equilibrium is stable, the upper equilibrium is unstable. Above this unstable equilbrium, unlimited growth of membrane permeability takes place. Thus bistability can occur at the membrane segment level (**MS.II**).

Similarly to the previous model by the same author, there is no communication between membrane segments of one cell. Therefore the model falls into variant **SC.IV** (fig S.4**D**).

S.5.1.3 Feugier *et al.* (2005)

In Feugier et al. [2005], production of auxin depends on a dynamically modeled enzyme (S):

$$\frac{dS}{dt} = p(1 - \frac{A}{A_{eq}}) - \delta S \tag{S.26}$$

In which p is production of the enzyme, A_{eq} is the value of auxin for which the enzyme production becomes 0 and δ is decay of the enzyme. Setting $\frac{dS}{dt} = 0$ and filling it in in the auxin equation gives:

$$\frac{dA}{dt} = \epsilon\frac{p}{\delta}(1 - \frac{A}{A_{eq}}) + i_{pas} + i_{pin}P - eA \tag{S.27}$$

which gives the same auxin equilibrium line as our default auxin equation (eq S.3). The authors also test the effect of saturated efflux, which does not alter the model's self-organising potential in our analysis.

In this model, net efflux feeds back on k_{on}in 9 different manners, most of which fit into our overview of possible feedback functions (section S.2.3.2). In fig S.3 we indicate which possible combinations of auxin and PIN dynamics are studied in the Feugier et al. [2005] model. All of these give bistable membrane segments (variants **MS.II** and **MS.III**).

When these feedbacks are combined with a limiting PIN pool, they fall into category **SC.II**. If, instead, the PIN pool is unlimiting, the models behave like the **SC.IV** variant.

S.5.1.4 Feugier and Iwasa (2006)

In Feugier and Iwasa [2006], a similar model was used as in the previous paper by the same authors, although slight changes were implemented. The auxin dynamics are described by equation S.1 and thus give the auxin equilibrium line from equation S.3. Net efflux feeds back on k_{on} in a quadratic manner and an limiting PIN pool is assumed. Hence the PIN equation becomes (similar to eq Flux.2.b):

$$\frac{dP}{dt} = (k_{on_b} + k_{on_f}\theta(F)F^2)(P_{tot} - P) - k_{off}P \tag{S.28}$$

With k_{on_b} the basal exocytosis and k_{on_f} the flux-dependent exocytosis. The resulting PIN equilibrium line is given by eq Flux.2.b. Thus, the model behaves as variant **MS.III** (fig S.3**C**). As a result of the superlinear feedback function and the limiting PIN pool, the single cell level is polar (variant **SC.II**, fig S.4**B**).

In this second model, the authors add a "flux-bifurcator" in order to generate loop formation in veins. The additional effects of the flux-bifurcator on the 2-dimensional model behaviour are beyond the scope of our analysis.

S.5.1.5 Fujita and Mochizuki (2006)

Fujita and Mochizuki [2006] studied the stability of a simplified flux-based model. The auxin equation is given by equation S.1 and, thus, the auxin equilibrium line by equation S.3. In the model, flux feeds back on PIN localisation in a superlinear manner. The model is not mechanistic, in that the feedback of flux on PINs is not specific for certain cycling rates. The PIN equation is:

$$\frac{dP_0}{dt} = m\left(\frac{1}{1+\mathrm{e}^{-\alpha(F_0-\beta)}} + \frac{1}{P_{tot}}\left(\frac{1}{1+\mathrm{e}^{-\alpha(F_0-\beta)}} + \frac{1}{1+\mathrm{e}^{-\alpha(F_1-\beta)}}\right)P_0\right) \tag{S.29}$$

In which m is the growth rate, F_0 and F_1 are fluxes over the two membrane segments of one cell (given by equation S.9), respectively, and α and β are constants determining the shape of the feedback. The resulting PIN equilibrium line is given by (which for reasons of simplicity we write for A as a function of P) (similar to eq Flux.3.b):

$$A = \frac{1}{\alpha e}\left((i_{pas} + i_{pin}P - \beta)\alpha + \ln\left(\frac{(P_{tot}-P)\mathrm{e}^{\alpha(-F_1+\beta)} + P_{tot} - 2P}{P}\right)\right) \tag{S.30}$$

This line is able to intersect three times with the auxin equilibrium line, thus bistability occurs at the membrane segment level (similar to **MS.III**, fig S.3**C**). Similar to the Smith et al. [2006] model, this PIN equilibrium line can shift to the right or left due to changes in the context of the cell and so lose its bistability.

Due to the finite PIN pool, that is at all times divided between P_0 and P_1, there is polarity at the single cell level (variant **SC.II**, fig S.4**B**).

S.5.1.6 Alim and Frey (2010)

Alim and Frey [2010] use the same assumptions as Feugier and Iwasa [2006] (in our analysis, disregarding the flux-bifurcator), i.e. the PIN pool is limiting and PIN exocytosis depends superlinearly on the flux (PIN equilibrium line Flux.2.b). Hence, the Alim and Frey [2010] model belongs to membrane segment variant **MS.III** and single cell variant **SC.II** (fig S.3**C** and S.4**B**).

S.5.2 Concentration based models

S.5.2.1 Jönsson *et al.* (2006)

The model constructed by Jönsson et al. [2006] is a concentration-based model used to simulate phyllotaxis. In this model auxin in the neighbouring cells feeds back on the PIN localisation at the membrane segments and membrane segments compete for a limiting PIN pool. Auxin transport is non-saturating. The authors apply two different feedback functions, a linear one and a superlinear, saturating one (where $k_{on} = \frac{A^3}{h^3+A^3}$). The linear feedback function is used for analysis on spacing of peaks. In this case, it is assumed that the PIN dynamics are in equilibrium and that all PINs recide on the membrane. Hence the PIN equilibrium line is given by:

$$P = \frac{P_{tot}A}{\sum_i^n A_i} \tag{S.31}$$

Additionally, when studying a 1D file, the authors assume that the pumping of auxin by PINs is linear. Therefore, the auxin equilibrium line is given by eq S.3. These equilibrium lines can only intersect once, hence the linear feedback does not allow for bistable behaviour at the membrane segment level (variant **MS.I**, fig S.3**A**). The superlinear, saturating feedback that is used for the 2-dimensional simulations, introduces non-linearity into the PIN equilibrium line and therefore does allow for bistable behaviour (variant **MS.III**, fig S.3**C**).

The linear feedback, combined with linear pumping, does not give cell polarity at the single cell level (variant **SC.I**, fig S.4**A**), whereas the superlinear, saturating feedback, combined with saturated pumping, does (variant **SC.II**, fig S.4**B**).

Interestingly, our tissue level analysis does show self-organised behaviour for the linear feedback function and linear pumping that does not give bistability or cell polarity. To further investigate this alternative Turing-like self-organising behaviour, we performed a bifurcation analysis on a 1-dimensional five cell model, consisting of 5 auxin and 10 PIN equations, specifically focusing on the parameter regions for which the cells in the tissue become polarised. Fig S.5 shows a bifurcation diagram of how the tissue level equilibria in a ring of five cells depend on the parameters P_{tot} and k_{off} for the Jönsson et al. [2006] model and a modified model that does not have a limiting PIN pool (eq Conc.3.a with $n = 1$). In order to obtain insight in whether polar equilibria occur, we introduce the variance (V) which reflects the difference in PIN levels on opposing membranes. Furthermore, to test for consistent polarisation among all 5 cells of the tissue, we sum these differences across cells. Thus, a large variance implies the presence of a strongly polar equilibrium in all cells of the tissue, whereas a variance of 0 implies that all cells are apolar. Variance is thus formally defined as:

$$V = \sum (P_{i,0} - P_{i,1})^2 \quad \text{with } i = 1, 2, 3, 4, 5 \tag{S.32}$$

For the Jönsson et al. [2006] model we see that, above a critical P_{tot} and below a critical k_{off} value, a bifurcation occurs that leads to a situation with persistenly polarised cells across the tissue. In contrast, no such behaviour was found for the alternative model without a limiting PIN pool. We therefore conclude that the limiting PIN pool is required to obtain the self-organising behaviour found in the Jönsson et al. [2006] model.

S.5.2.2 Merks *et al.* (2007)

In the concentration-based model by Merks et al. [2007], efflux of auxin through the PINs saturates. The authors do not take into account production and decay of auxin in all cells, but allow auxin to flux into the tissue from a source and to leave it through a sink. Again, we approximate this global production and decay with local, cellular production and decay processes. Therefore we can use equation S.2 for the auxin which provides the auxin equilibrium line in eq S.4.

In contrast to other models in which a limiting PIN pool is assumed, the authors describe the cytosolic PINs (P_c) dynamically:

$$\frac{dP_c}{dt} = p_{pin} - d_{pin}P_c + k_{off} \sum P_i - \sum \frac{k_{on}P_c}{k_m + P_c} \tag{S.33}$$

In which p_{pin} is the production of PINs, whereas d_{pin} is the decay rate. Endocytosis as well as exocytosis are summed over all membrane segments of the cell. The exocytosis rate saturates with the amount of PINs in the cytosol and the half-maximum rate is obtained when $P_c = k_m$.

At the membrane segment level, P is described as:

$$\frac{dP_i}{dt} = \frac{k_{on}P_c}{k_m + P_c} - k_{off}P_i \tag{S.34}$$

k_{on} depends on auxin in a saturating manner:

$$k_{on} = \frac{k_{on_f}A}{h_A + A} \tag{S.35}$$

Setting equation S.33 to 0, given only one membrane segment ($\sum P_i = P$) and assuming that PIN production and decay are in equilibrium gives us a measure for P_c. Filling this and k_{on} from equation S.35 into equation S.34

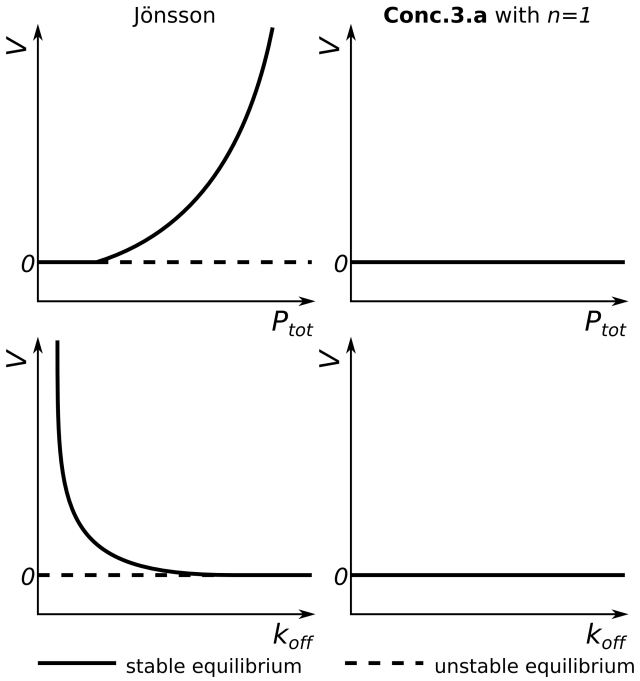

Figure S.5: Bifurcation diagrams for a ring of cells in the Jönsson et al. [2006] model and eq Conc.3.a with $n = 1$. Dependence of variance V on P_{tot} (upper panels) and k_{off} (lower panels). The Jönsson et al. [2006] model shows stable equilibria in which $V > 0$ and, thus, permanent tissue polarisation occurs. The model with eq Conc.3.a with $n = 1$ has only one equilibrium for $V = 0$. Hence, no polarity is found.

and setting the resulting $\frac{dP}{dt}$ equation to 0 provides the following PIN equilibrium line (similar to eq Flux.3.b) for P at the membrane segment:

$$P = \frac{p_{pin} k_{on_f} A}{k_{off}(p_{pin} A + d_{pin} k_m A + p_{pin} h_A + d_{pin} k_m h_A)} \tag{S.36}$$

This line can intersect thrice with the auxin equilibrium line (fig S.3**D**), therefore bistability can occur at the membrane segment level (variant **MS.IV**).

The single cell phase plane is shown in fig S.4**D**. In this model PIN concentrations change not only due to exo- and endocytosis, but also due to production and decay of PINs. It is noteworthy that decay of PINs occurs only for cytosolic but not for membrane bound PINs. As a result, although the cytosolic PIN pool has a fixed equilibrium size, the total amount of PINs that a cell contains is not fixed, but varies with the amount that is present on the membrane segments. As a consequence, the PIN pool in this model is effectively unlimiting, as can be seen from the additional bipolar equilibrium at the single cell level. Hence, the model falls into single cell category **SC.IV**.

S.5.2.3 Newell *et al.* (2007)

For their combined concentration- and physical force-based model, Newell et al. [2007] used the PIN and auxin equations first described by Jönsson et al. [2006] for the 1D cell file (linear feedback, linear auxin transport) and translated these into continuous equations. However, they did not study the model with a QSS assumption for the PIN cycling and did not assume that all the PINs reside on the membrane as done by Jönsson et al. [2006]. The auxin equilibrium line is given by eq S.3 and the PIN equilibrium line is given by eq Conc.1.b. As a result, the model is not bistable at the membrane segment level (variant **MS.I**, fig S.3**A**) and not polar at the single cell level (variant **SC.I**, fig S.4**A**). However, due to the limiting PIN pool and up-the-gradient PIN polarisation, this model is still able to self-organise at the tissue level, similar to the Jönsson et al. [2006] model with linear feedback and non-saturated auxin transport.

S.5.2.4 Sahlin *et al.* (2009)

Sahlin et al. [2009] developed a concentration-based model for phyllotaxis. They include apolar expression of AUX1, which cannot be included in our framework, because we do not explicitly model the cell wall. Auxin transport is saturated for high auxin concentrations, hence the auxin equilibrium line is given by eq S.4. The PIN pool is limiting, and several feedback functions have been used. The most simple feedback function is linear which, combined with the limiting PIN pool gives the PIN equilibrium line in eq Conc.1.b. Due to the combination of the non-linear auxin equilibrium line and the non-linear PIN equilibrium line, the model is bistable at the membrane segment level (variant **MS.IV**). At the single cell level, polarity occurs (variant **SC.II**).

S.5.3 Joined concentration- and flux-based model

Bayer et al. 2009 Bayer et al. [2009] incorporated both up-the-gradient and with-the-flux PIN polarisation into their model. Cells in the model apply one of these two mechanisms, deciding which one based on their auxin level. The auxin equation is the same as used in their previous model [Smith et al., 2006], which is described in the main text. The authors assume a limiting PIN pool at the single cell level and saturated transport of auxin (with co-operativity 2).

In the up-the-gradient feedback regime the model is identical to the [Smith et al., 2006] model. It thus falls into category **MS.III** at the membrane segment and shows bistable behaviour (fig S.3**C**). At the single cell level, the model is polar (variant **SC.II**, fig S.4**B**).

In the with-the-flux regime, the authors apply the same shape of feedback function, but substitute auxin concentration with a new variable "flux history" that depends on the net efflux (similar to eq Flux.3.b):

$$P = \frac{P_{tot} b^F}{\sum_n b^{F_i}} \tag{S.37}$$

in which b is a base parameter that the authors set to 2 or 3 and the sum is taken over the fluxes over all membrane segments. The resulting PIN equilibrium line has a superlinear saturating shape that can intersect three times with the auxin equilibrium line given by eq S.4 (variant **MS.III**, fig S.3**C**). Hence, also in the with the flux regime, the model supports membrane bistability, and cell polarity (variant **SC.II**, fig S.4**B**).

P_{tot} is calculated dynamically, as in the model by [Smith et al., 2006], however, since all the PINs are assumed to be on the membrane, these models do not have the issue described for the model by Merks et al. [2007], namely that the PIN pool is effectively unlimited.

S.5.4 Mechanistic models

Heisler et al. 2010 In the model by Heisler et al. [2010], PIN localisation is determined by wall stress which in turn is dependent on auxin concentrations within neighbouring cells. Active transport of auxin is saturated, therefore the auxin dynamics are determined by equation S.2 and the corresponding auxin equilibrium line is given by equation S.4. As in their previous model [Jönsson et al., 2006], the authors assume that PIN dynamics are at all times in equilibrium and that all PINs reside on the membrane. They write the following dependency of PINs on the membrane stresses experienced by a membrane segment:

$$P = \frac{P_{tot} k_2 s^n}{1 + \sum k_2 s_i^n} \tag{S.38}$$

in which P_{tot} is the total amount of PINs in a cell, s is the stress experienced by a single membrane segment, k_2 is the level by which PINs depend on the stress and n is the co-operativity with which this happens. The sum is taken over all the membrane segments belonging to one cell. For a single membrane segment, we can write:

$$P = \frac{P_{tot} k_2 s^n}{1 + k_2 s^n + k_2 h^n} \tag{S.39}$$

In which h represents the stresses experiences by the other membrane segments that are not in focus and thus assumed to be constant. The stress negatively depends on wall elasticity as follows:

$$s = \frac{F}{A_0(1 + \frac{E(A)}{E(A_i)})} \tag{S.40}$$

F is the isotropic force on each wall, A_0 is the cross section of a cell and A_i is the auxin content of the cell to which the membrane segments belongs and is thus assumed to be constant. $E(A)$ is the wall elasticity which is a function of auxin in the neighbouring cell:

$$E = E_{min} + \frac{(E_{max} - E_{min}) k_3^m}{A + k_3^m} \tag{S.41}$$

E_{min} is the minimal and E_{max} the maximal wall elasticity. E decreases with auxin. k_3 is a saturation constant and m is the co-operativity with which elasticity depends on auxin. The full PIN equilibrium line is obtained by substituting S.40 and S.41 into S.39 Because of its length and complexity we refrain from giving it explicitly. However, for the parameters used by the authors, it can be shown to describe a sublinear, saturating, function (similar to eq Conc.3.a). However, considering that the auxin equilibrium line is also a non-linear line, this should theoretically allow for three intersection points between the equilibrium lines and thus the model falls into membrane segment category **MS.IV** (fig S.3**D**). In line with this and because of the limiting PIN pool, we expect polarity at the single cell level (variant **SC.II**, fig S.4**B**).

Wabnik et al. 2010 Wabnik et al. [2010] developed a PAT model in which auxin in the cell wall, by binding to a receptor, inhibits endocytosis of PINs from the nearest membrane. In order to study this model, we extended our framework to include the cell wall. In our membrane segment model, A is the concentration of auxin in the neighbouring cell. For this model, we use A for the concentration of auxin in the cell wall adjoining the membrane segment of interest. The dynamics are the same, the cell wall receives auxin by active and passive transport over

the membrane segment of interest and it loses auxin by influx. Hence, we can use the same equation that we used for auxin in the neighbouring cells for saturated efflux (equation S.2 and corresponding equilibrium line S.4).

Similar to Merks et al. [2007], the authors model the cellular PIN pool dynamically, in this case, however, feedback is implemented through the endocytosis rate k_{off}. The cytosolic PIN pool is given by:

$$\frac{dP_c}{dt} = p_{pin} - d_{pin}P_c + \sum_n k_{pin}P_i - \sum_n k_{on}P_c \tag{S.42}$$

In which the sums are taken over all membrane segments belonging to one cell.

The equation for PINs on the membrane segment is:

$$\frac{dP}{dt} = k_{on}P_c - k_{off}P \tag{S.43}$$

For the formation of complexes (C) between auxin and receptor in the cell wall, we use, as in the original publication, a QSS assumption. Thus allows us to write

$$C = \frac{2r_T A}{2k_d + \sum_n A_i} \tag{S.44}$$

In which r_T is the total amount of receptors in the cell wall, k_d is a saturation constant and the sum is taken over all segments of the cell wall.

For the membrane segment level, since we assume auxin concentrations to be constant in all compartments other than the cell wall segment of interest, we can rewrite eq S.44 as:

$$C = \frac{2r_T A}{2k_d + h + A} \tag{S.45}$$

In which h now represents the auxin concentrations in other cell wall compartments. The endocytosis rate of PINs now depends on the amount of complex as such:

$$k_{off} = k_{off_b} + \frac{k_{off_f}}{1 + C} \tag{S.46}$$

The PIN equilibrium line that is obtained by substituting equation S.46 and S.45 into S.43 is a saturating, sublinear function. Hence, it can intersect more than once with the non-linear auxin equilibrium line and there is bistability at the membrane segment level (variant **MS.IV**, fig S.3**A**).

For the single cell level, as in Merks et al. [2007], the PIN pool in the Wabnik et al. [2010] model increases with the amount of PINs that are on the membrane. Therefore, it is effectively unlimiting. There is, however, still a slight effect of P_0 on P_1 and *vice versa*, therefore the PIN equilibrium lines are not completely horizontal and vertical and the model belongs to category **SC.IV**.

To study the tissue behaviour, we extended the framework to include cell walls. We found that the model is able to self-organise after a perturbation is provided to one of the cells. The resulting PIN polarisation is similar to with-the-flux models, where the PINs point from the source to the sink in a cell file, and all point in the same direction in a ring of cells. In order to obtain this behaviour, auxin diffusion in the cell wall must be sufficiently low, to allow for the formation of an auxin gradient. Therefore, it appears that the model's self-organising behaviour relies on across-cell wall polarity as well as cell polarity.

References

K Alim and E Frey. Quantitative predictions on auxin-induced polar distribution of PIN proteins during vein formation in leaves. *The European Physical Journal E*, 33:165–173, 2010.

EM Bayer, RS Smith, T Mandel, N Nakayama, M Sauer, P Prusinkiewicz, and C Kuhlemeier. Integration of transport-based models for phyllotaxis and midvein formation. *Genes and Development*, 23(3):373–384, 2009.

FG Feugier and Y Iwasa. How canalization can make loops: A new model of reticulated leaf vascular pattern formation. *Journal of Theoretical Biology*, 243(2):235–244, 2006.

FG Feugier, A Mochizuki, and Y Iwasa. Self-organization of the vascular system in plant leaves: Inter-dependent dynamics of auxin flux and carrier proteins. *Journal of Theoretical Biology*, 236(4):366–375, 2005.

H Fujita and A Mochizuki. Pattern formation of leaf veins by the positive feedback regulation between auxin flow and auxin efflux carrier. *Journal of Theoretical Biology*, 241:541–551, 2006.

MG Heisler, O Hamant, P Krupinski, M Uyttewaal, C Ohno, H Jönsson, J Traas, and EM Meyerowitz. Alignment between PIN1 polarity and microtubule orientation in the shoot apical meristem reveals a tight coupling between morphogenesis and auxin transport. *PLoS Biology*, 8(10), 2010.

H Jönsson, MG Heisler, BE Shapiro, EM Meyerowitz, and E Mjolsness. An auxin-driven polarized transport model for phyllotaxis. *Proceedings of the National Academy of Sciences of the United States of America*, 103(5): 1633–1638, 2006.

RMH Merks, Y Van de Peer, D Inzé, and GTS Beemster. Canalization without flux sensors: a traveling-wave hypothesis. *Trends in Plant Science*, 12(94):384–390, 2007.

GJ Mitchison. A model for vein formation in higher plants. *Proceedings of the Royal Society of London - Biological Sciences*, 207(1166):79–109, 1980.

GJ Mitchison. The polar transport of auxin and vein patterns in plants. *Phil. Trans. R. Soc. Lond.*, 295:461–471, 1981.

AC Newell, PD Shipman, and Z Sun. Phyllotaxis: cooperation and competition between mechanical and biochemical processes. *Journal of Theoretical Biology*, 251:421–439, 2007.

P Sahlin, B Söderberg, and H Jönsson. Regulated transport as a mechanism for pattern generation: Capabilities for phyllotaxis and beyond. *Journal of Theoretical Biology*, 258(1):60–70, 2009.

RS Smith, S Guyomarc'h, T Mandel, D Reinhardt, C Kuhlemeier, and P Prusinkiewicz. A plausible model of phyllotaxis. *Proceedings of the National Academy of Sciences of the United States of America*, 103(5):1301–1306, 2006.

K Wabnik, J Kleine-Vehn, J Balla, M Sauer, S Naramoto, V Reinöhl, RM Merks, W Govaerts, and J Friml. Emergence of tissue polarization from synergy of intracellular and extracellular auxin signaling. *Molecular Systems Biology*, 6(447), 2010.